Supporting Information

Iron[III]-Complexes with *N*-Phenylpyrazole-based Ligands

Tanja Hirschhausen1†, Lorena Fritsch1†, F. Lux [1], J. Steube[1], R. Schoch [1], A. Neuba [1], H. Egold[1] and M. Bauer [1,2]*

[1]   Institute of Inorganic Chemistry, Paderborn University, Paderborn, Germany.
[2]   Center for Sustainable Systems Design, Paderborn University, Paderborn, Germany
*   Correspondence: matthias.bauer@upb.de
†   These authors contributed equally to this work.

Contents

General procedure

Synthesis of ligands and complexes were carried out under standard Schlenk conditions, under inert and anhydrous conditions. Inert and pre-dried argon was used, and all applied glass wear was heated and re-filled with argon at least three times. Water free solvents were provided by a solvent drying-plant by MBraun (MB SPS 800) and purged with argon prior use. Used chemicals for all synthesis were commercially purchased by the following providers*: Fischer Scientific, Merck, Abcr*, and *TCI*, and used without further purification. Ligand synthesis has been reported in literature.[1,2]

NMR spectra were recorded on a BRUKER Avance 700 (^{1}H, 700.1 MHz) using deuterated solvents by *Deutero* without further purification. NMR signals were referred to residual solvent signals relative to TMS. Mass spectrometry was measured with a quadrupol time-of-flight mass spectrometer (MS) Synapt 2G by the company WATERS. Elemental analysis measurements were performed with a Micro Cube by ELEMENTAR and were compared with the theoretical calculated mass. A **PerkinElmer** Lambda 465 single beam spectrophotometer was used for Uv-Vis spectra. Concentrations contained a 10^{-5} M complex solution in BuCN, and were filled in a **Hellma** quartz cuvette with a pathlength of 1 cm. For IR spectroscopy a Bruker Vertex 70, with the sample as solid powder and the ATR-technique, was applied. Cylovoltagramms were measured with a 10^{-3} M analyte and 0.1 M [*n*-Bu$_4$N](PF$_6$) concentration on

a PGSTAT 101 potentiostat from **Metrohm-Autolab**. Emission spectra were recorded on a FLS1000 from **Edinburgh Instruments** at room-temperature.

General procedure of complex synthesis

Under Argon atmosphere respective ligand (3 equiv) was suspended in tetrahydrofuran (THF) (10 mL). Ethylmagnesium bromide (4 equiv, 0.9 M in THF) was added dropwise and refluxed overnight. In a second round button flask, iron powder (12 equiv) was added to THF solution of iron(II) bromide (1.5 equiv) (40 mL) and refluxed overnight. After refluxing, the flask was cooled to room-temperature and the ligand-solution was cooled in an ethanol-nitrogen bath to -80°C. The iron(II) bromide solution was added dropwise and slowly warmed to room temperature under an argon atmosphere. To the reaction mixture a solution of NH_4Cl (100 mL, 15 g/L) was added, and extracted with dichloromethane (DCM) (3x100 mL). The combined organic portions were dried with $MgSO_4$ and concentrated under reduced pressure. Column chromatography with silica as solid phase and DCM as eluent was applied. The combined fractions were concentrated under reduced pressure and crystallized with slow diffusion of cyclopentane into the DCM-analyte solution. After removing the crystalline product and drying at 50°C at high vacuum, the compound was received as elemental analysis pure product.

Fe(ppz)$_3$

The complex was obtained as yellow powder (7.5%)

^{1}H-NMR (700.0 MHz, CD$_3$CN): δ = -75.20 (s, 1H, 2-*H*), -9.27 (s, 1H, 9-*H*), -5.25 (s, 1H, 4-*H*), -3.35 (s, 1H,8-*H*), -1.15 (s, 1H, 5-*H*), 7.90 (s, 1H, 3-*H*), 13.04 (s, 1H, 7-*H*) ppm.

^{13}C-NMR (176.1 MHz, CD$_3$CN): δ = -92.7 (1C, 3-*C*), -74.8 (1C, 5-*C*), 100.2 (1C, 7-*C*), 117.0 (1C, 8-*C*), 122.9 (1C, 9-*C*), 239.9 (1C, 4-*C*), 389.1 (1C, 2-*C*), 396.6 (1C, 6-*C*) ppm.

^{15}N-NMR (70.96 MHz, CD$_3$CN): 70.4 ppm. (ESI in MECN): m/z 485.1160 (for C$_{27}$H$_{21}$FeN$_6$ calc. 485.1177)

Elemental analysis: calc. for C$_{27}$H$_{21}$FeN$_6$ C: 66.82%, H: 4.36%, N: 17.32%, found: C: 66.77%, H: 4.56%, N: 17.25%.

IR (ATR, $\tilde{\upsilon}$ [cm^{-1}]): 3139w, 3041w, 1573w, 1506w, 1461m, 1434m, 1417m, 1398m, 1328w, 1270m, 1236w, 1193w, 1153w, 1099w, 1064m, 1043m, 1012m, 960m, 918w, 871w, 825w, 742s, 715m, 698m, 661w, 644w, 609m.
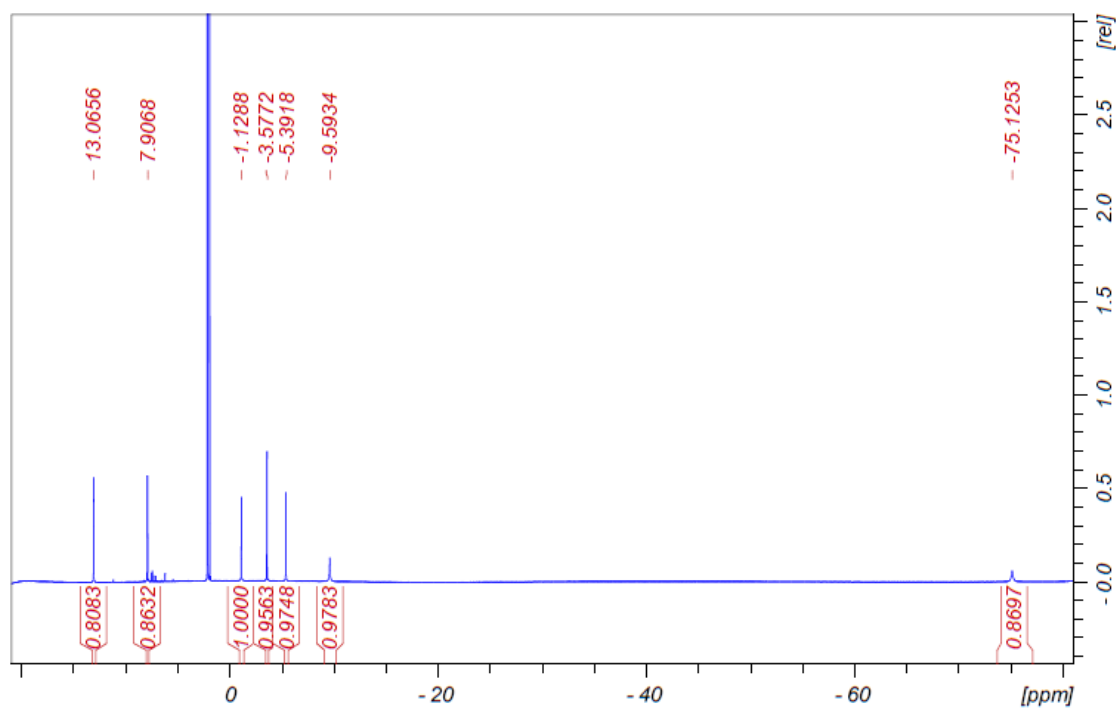
Figure S1: ^{1}H-NMR spectrum of complex Fe(ppz)$_3$ in CD$_3$CN
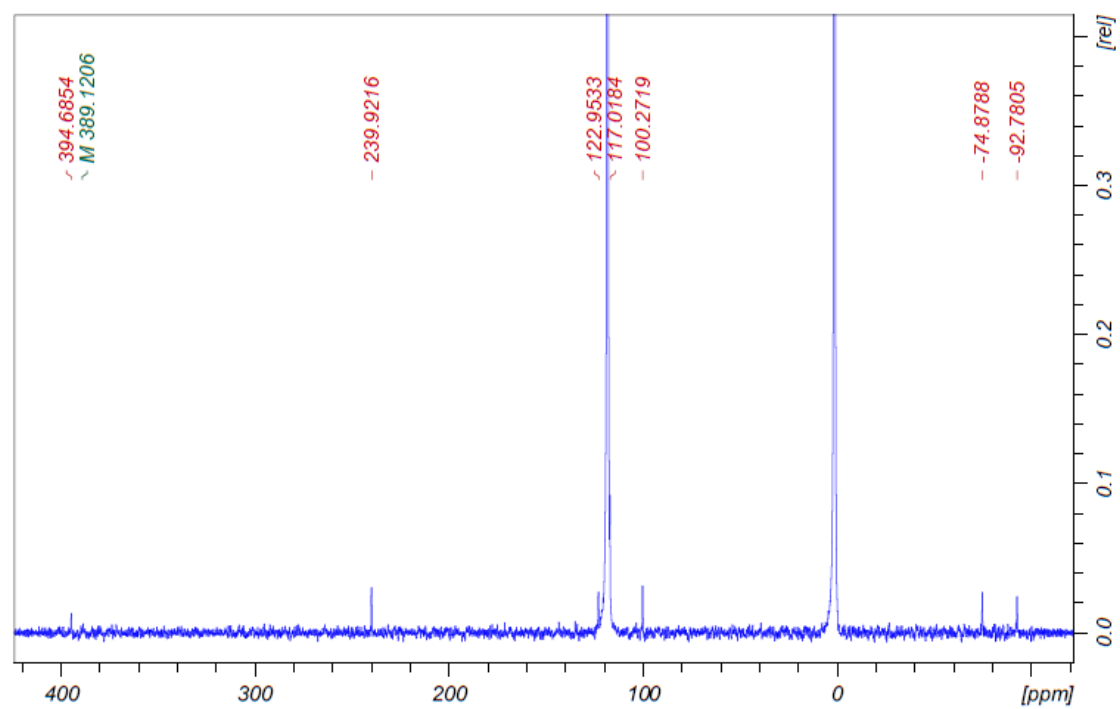
Figure S2: ^{13}C-NMR spectrum of complex Fe(ppz)$_3$ in CD$_3$CN

3
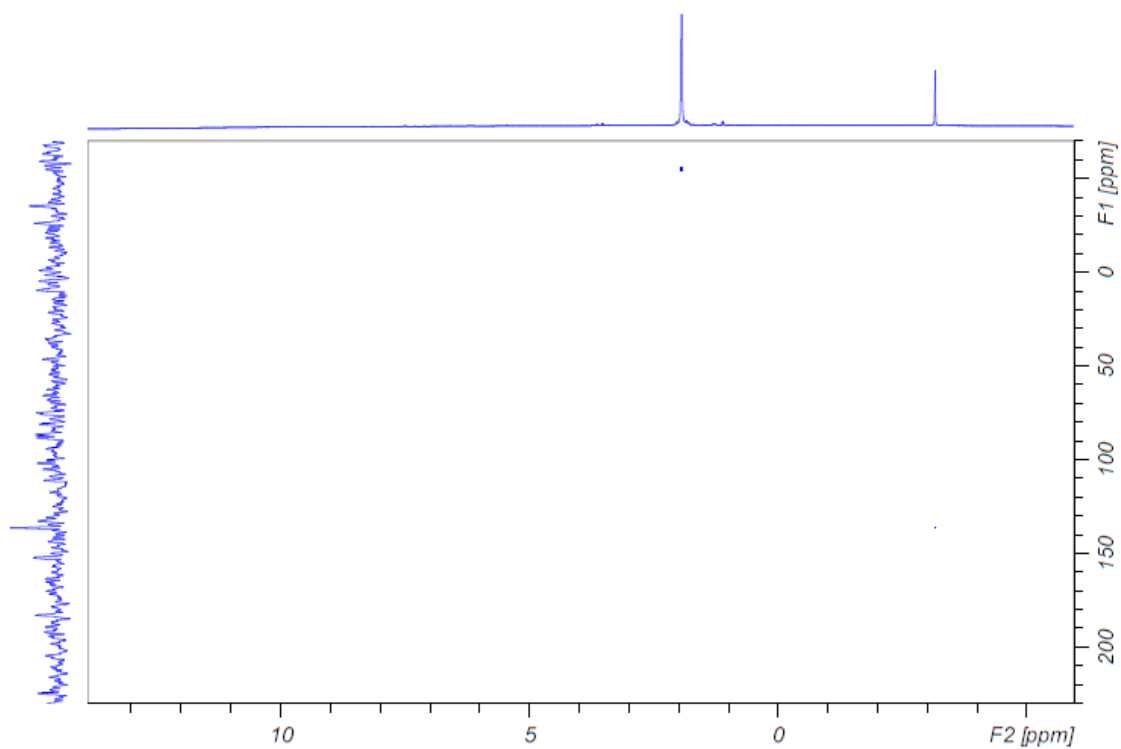
**Figure S3:** ^{15}N-HMBC spectrum of Fe(ppz)$_3$ in CD$_3$CN, second signal is the folded signal of non-deuterated solvent CH$_3$CN
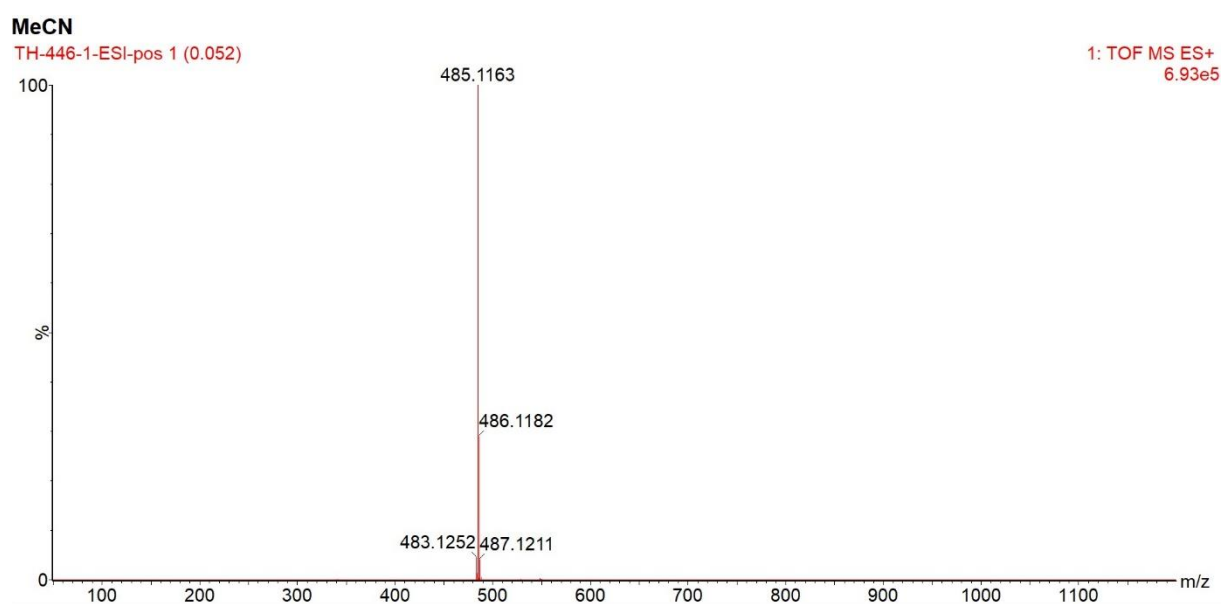
Figure S4: ESI-MS spectrum of complex Fe(ppz)$_3$ in CH$_3$CN
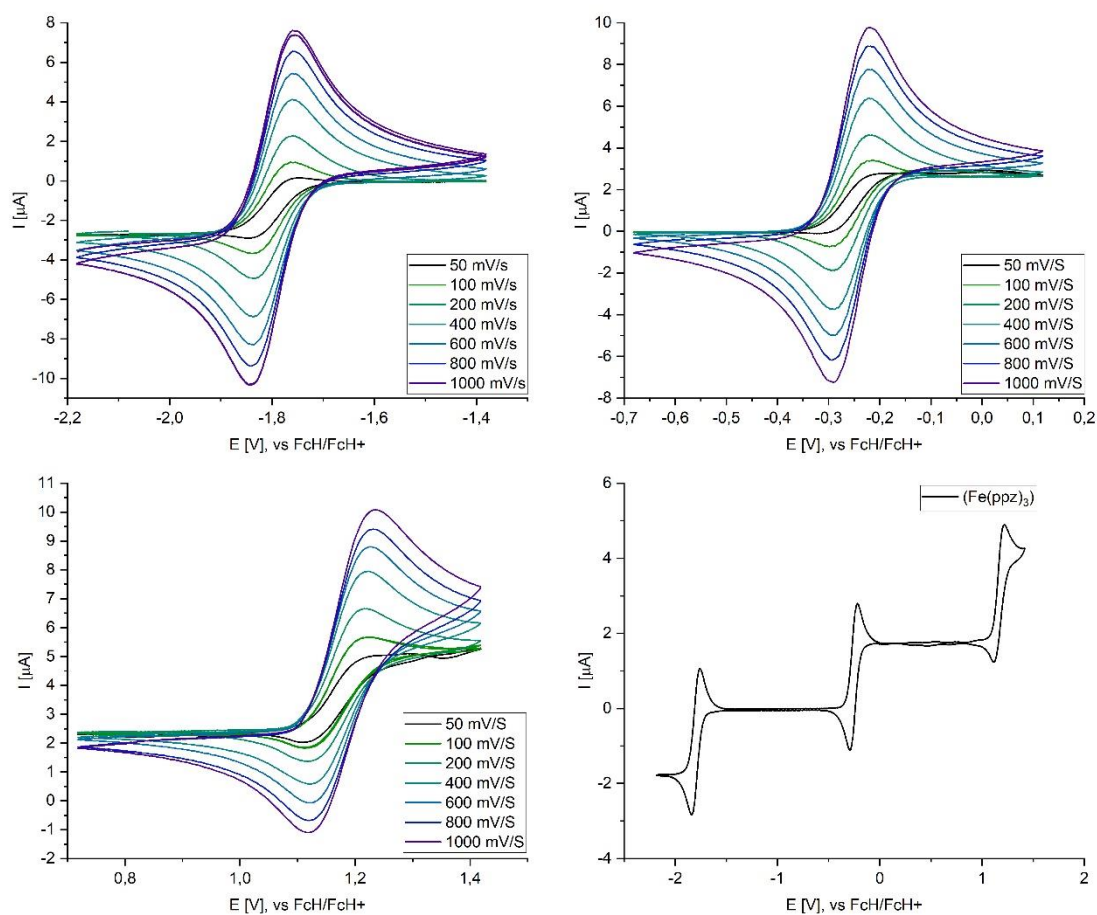
Figure S5: Complete cyclovoltammetry spectra for complex Fe(ppz)$_3$ in CH$_3$CN

Table S1: Cyclovoltammetry data for Fe(ppz)$_3$ at different scan rates, first redox step

SCANRATE	[MV/S]	50	100	200	400	600	800	1000
E_{PC}	[V]	-1,835	-1,828	-1,833	-1,835	-1,835	-1,840	-1,838
E_{PA}	[V]	-1,762	-1,765	-1,759	-1,762	-1,760	-1,760	-1,762
$E_{1/2}$	[V]	-1,80	-1,80	-1,80	-1,80	-1,80	-1,80	-1,80
ΔE	[V]	0,073	0,063	0,074	0,073	0,076	0,081	0,076
I_{PA}	[µA]	-1,68	-2,73	-4,11	-5,76	-7,11	-8,17	-9,07
I_{PC}	[µA]	1,64	2,78	4,11	5,87	7,14	8,24	9,14
I_{PA}/I_{PC}		-0,98	-1,02	-1,00	-1,02	-1,00	-1,01	-1,01
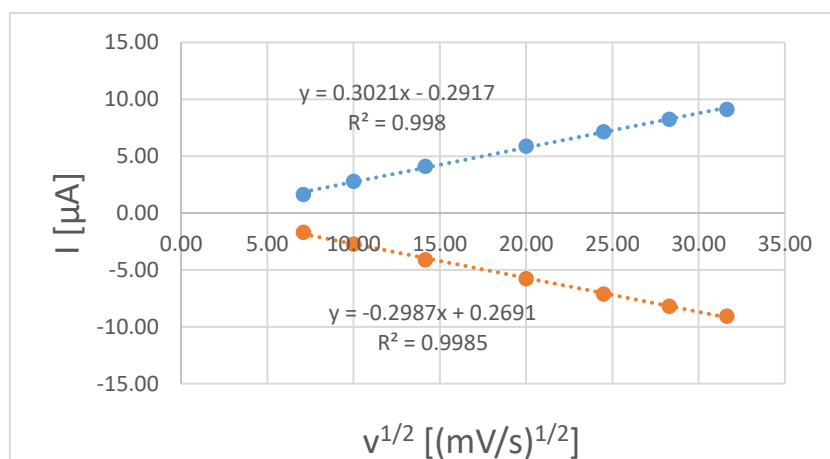
Figure S6: Plotted data of Randles-Sevcik-Equation Fe(ppz)$_3$ at different scan rates, first redox step

**Table S2:** Cyclovoltammetry data for Fe(ppz)$_3$ at different scan rates, second redox step

SCANRATE	[MV/S]	50	100	200	400	600	800	1000
E_{PC}	[V]	-0,296	-0,286	-0,289	-0,289	-0,289	-0,294	-0,291
E_{PA}	[V]	-0,223	-0,225	-0,223	-0,223	-0,225	-0,223	-0,223
$E_{1/2}$	[V]	-0,26	-0,26	-0,26	-0,26	-0,26	-0,26	-0,26
ΔE	[V]	0,073	0,061	0,066	0,066	0,063	0,071	0,068
I_{PA}	[µA]	-1,88	-2,65	-3,80	-5,43	-6,88	-8,00	-9,00
I_{PC}	[µA]	1,55	2,41	3,80	5,53	6,69	7,79	8,72
I_{PA}/I_{PC}		-0,83	-0,91	-1,00	-1,02	-0,97	-0,97	-0,97
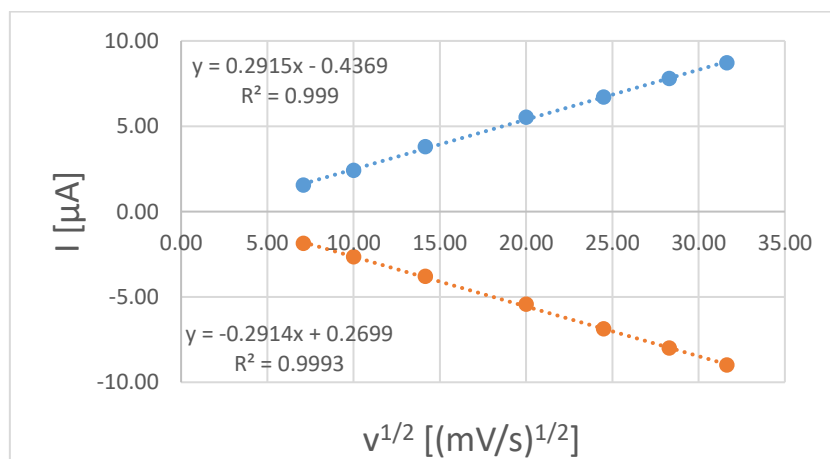
Figure S7: Plotted data of Randles-Sevcik-Equation Fe(ppz)$_3$ at different scan rates, second redox step

Table S3: Cyclovoltammetry data for Fe(ppz)$_3$ at different scan rates, third redox step

SCANRATE	[MV/S]	50	100	200	400	600	800	1000
E_{PC}	[V]	1,126	1,131	1,123	1,128	1,128	1,128	1,126
E_{PA}	[V]	1,211	1,209	1,209	1,216	1,216	1,221	1,226
$E_{1/2}$	[V]	1,17	1,17	1,17	1,17	1,17	1,17	1,18
ΔE	[V]	0,085	0,078	0,085	0,088	0,088	0,093	0,100
I_{PA}	[µA]	-1,70	-1,88	-2,77	-3,77	-4,57	-5,17	-5,73
I_{PC}	[µA]	1,35	2,02	2,92	3,97	4,64	5,12	5,52
I_{PA}/I_{PC}		-0,80	-1,08	-1,06	-1,05	-1,01	-0,99	-0,96
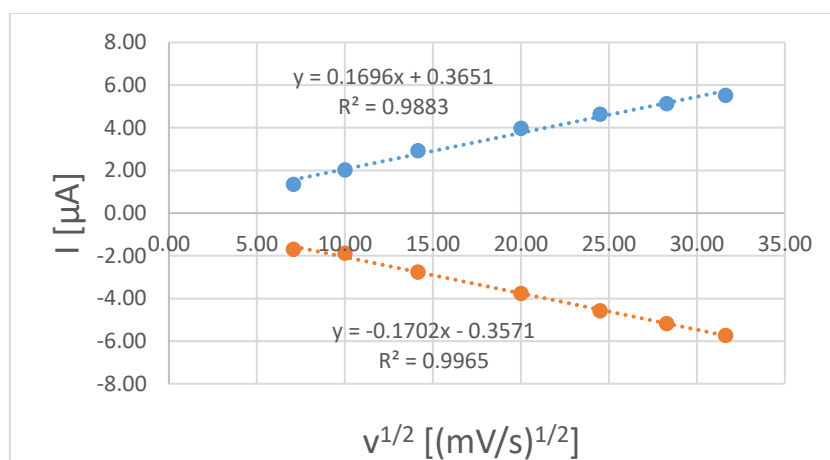
Figure S8: Plotted data of Randles-Sevcik-Equation Fe(ppz)$_3$ at different scan rates, third redox step
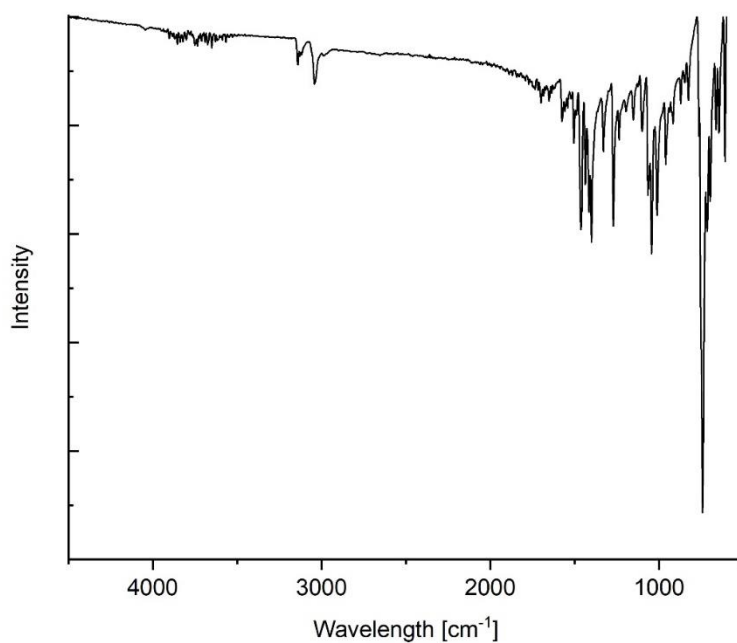
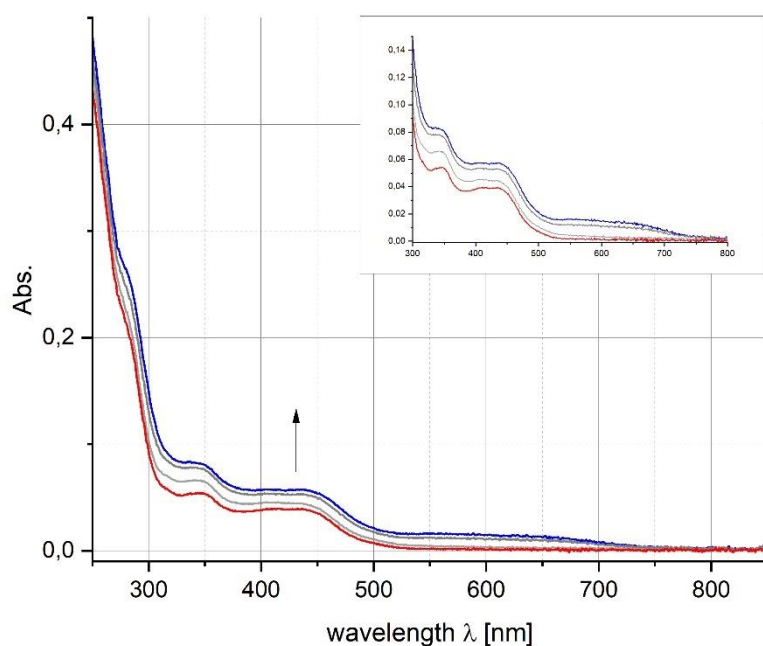**Figure S9:** ATR-IR spectrum for complex Fe(ppz)$_3$
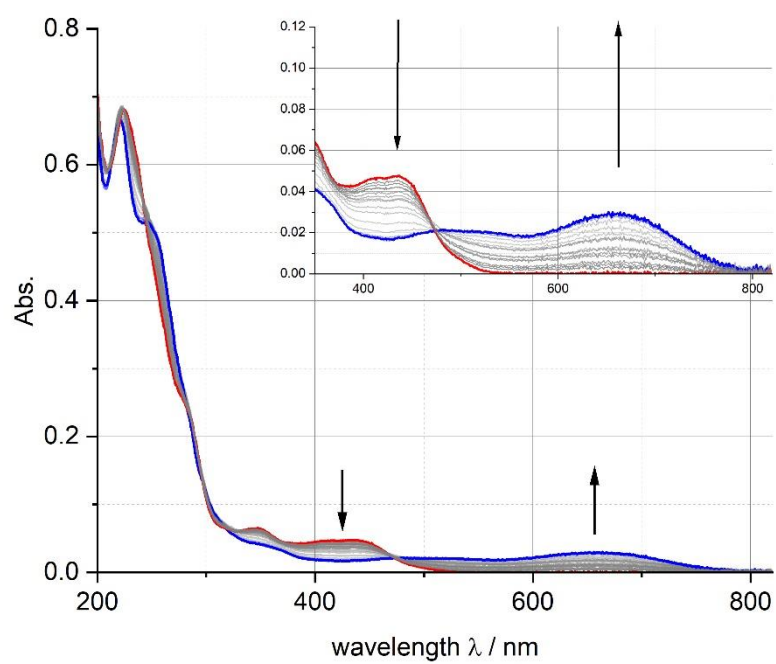
Figure S10: Change in the absorptive behaviour of Fe(ppz)$_3$ with an applied potential of 0.5-2 V in CH$_3$CN
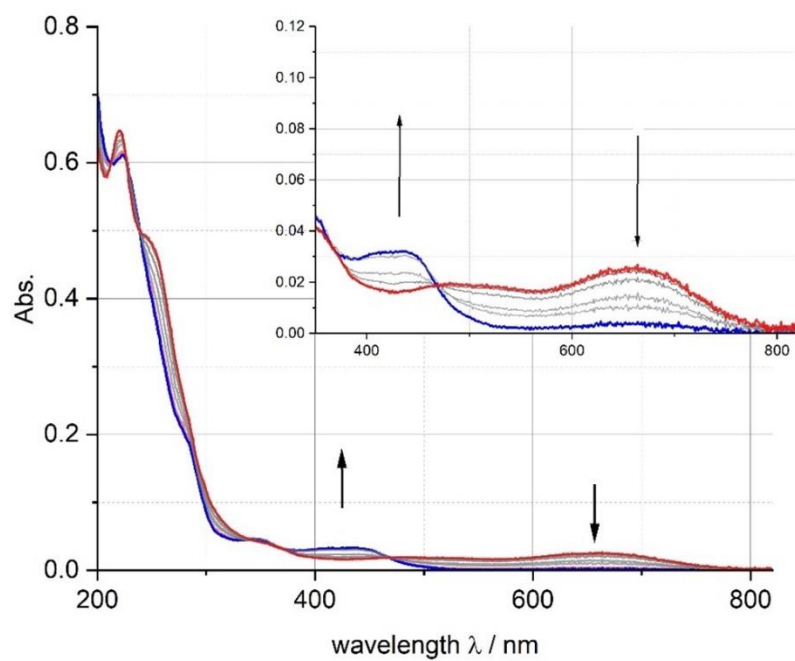
Figure S11: Change in the absorptive behaviour of Fe(ppz)$_3$ with an applied potential of -0.5 V in CH$_3$CN

Figure S12: Change in the absorptive behaviour of Fe(ppz)₃ with an applied potential of -2.0-2.5 V in CH₃CN

Fe(bppz)₃

The complex was obtained as red powder (3.9%).

¹H-NMR (700 MHz, CD$_3$CN): δ = -77.61 (1s, 1H, 2-*H*) -10.18 (s, 1H, 13-*H*), -4.64 (s, 1H, 8-*H*), -3.21 (s, 1H, 12-*H*), -1.74 (s, 1H, 9-*H*), 5.39 (d, $^3J_{HH}$ = 8.19 Hz, 2H, 5,5´-*H*), 5.75 (t, $^3J_{HH}$ = 7.60 Hz, 2H, 6,6´-*H*), 7.10 (t, $^3J_{HH}$ = 7.14 Hz, 1H, 6-H) 11.84 (s, 1H, 11-*H*) ppm.).

¹³C-NMR (176.1 MHz, CD$_3$CN): δ = -79.6 (1C, 152.5 Hz, 9-*C*), -77.9 (1C, 3-*C*), 105.4 (1C, 185.7 Hz, 11-*C*), 114.4 (1C, 62.3 Hz, 12-*C*), 115.3 (2C, 89.03 Hz, 5,5´-*C*), 123.1 (1C, 162.9 Hz, 7-*C*), 130.9 (2C, 160.4 Hz, 6,6´-*C*), 131.9 (1C, 183.3 Hz, 13-*C*), 154.1 (1C, 4-*C*), 241.4 (1C, 158.8 Hz, 8-*C*), 370.5 (1C, 133.9 Hz, 2-*C*), 396.7 (1C, 10-*C*) ppm.

¹⁵N-NMR (70.96 MHz, CD$_3$CN): 71.0 ppm.

MS (ESI in MECN): m/z 713.2150 (for C$_{45}$H$_{33}$FeN$_6$ calc. 713.6460).

Elemental analysis: calc. for C$_{45}$H$_{33}$FeN$_6$ C: 75.74%, H: 4.66%, N: 11.78%, found: C: 71.15%, H: 4.84%, N: 10.78%.

IR (ATR, $\tilde{v}$ [cm^{-1}]): 3108w, 3056w, 3020w, 1598w, 1564w, 1502w, 1465m, 1400m, 1373w, 1330w, 1261m, 1112w, 1064m, 1047m, 1016w, 958w, 916w, 894w, 808s, 757s, 734s, 694s, 663w, 649w, 607w.
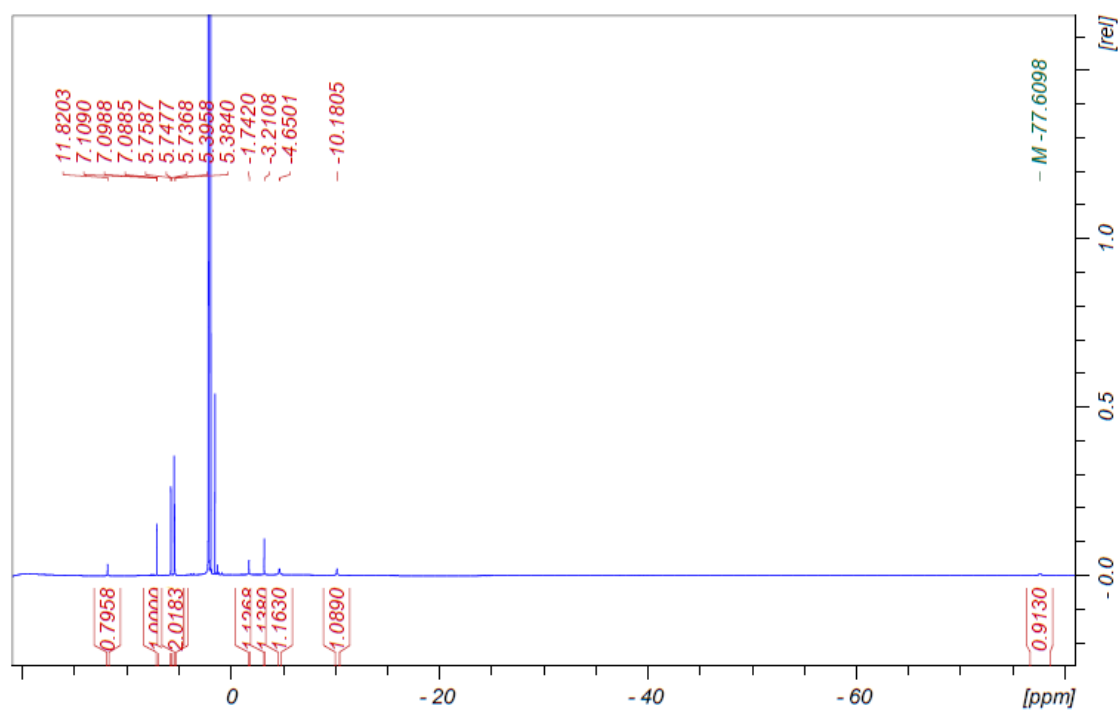
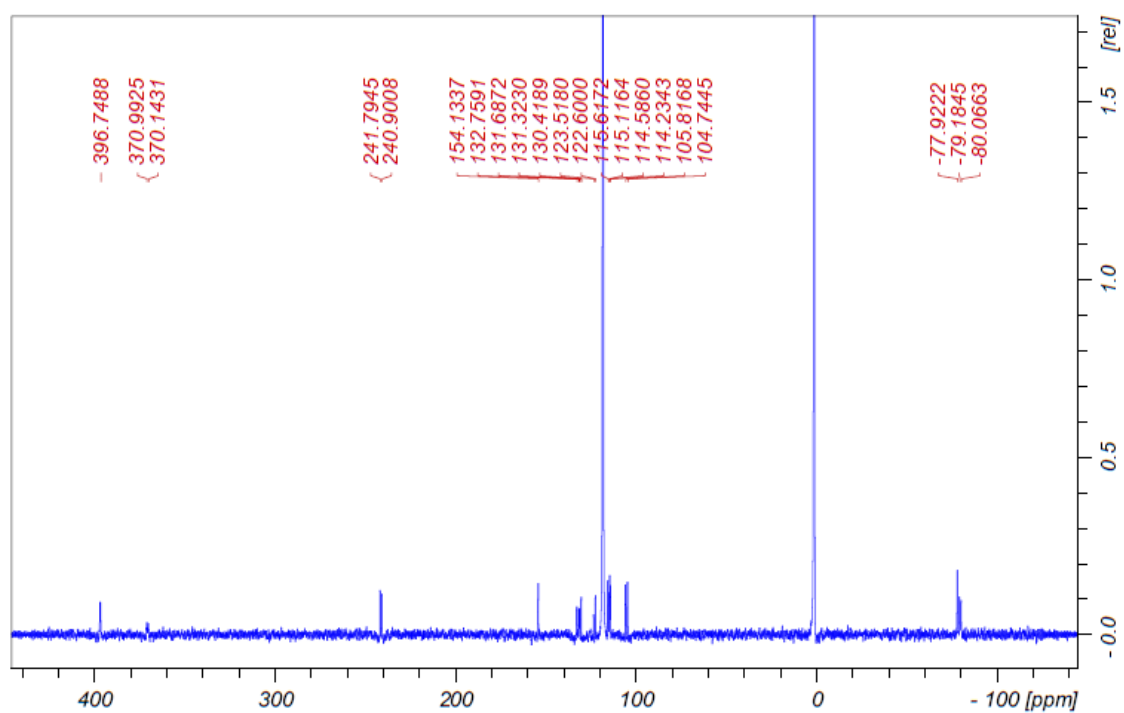**Figure S13:** ^{1}H-NMR spectrum of complex Fe(bppz)$_3$ in CD$_3$CN

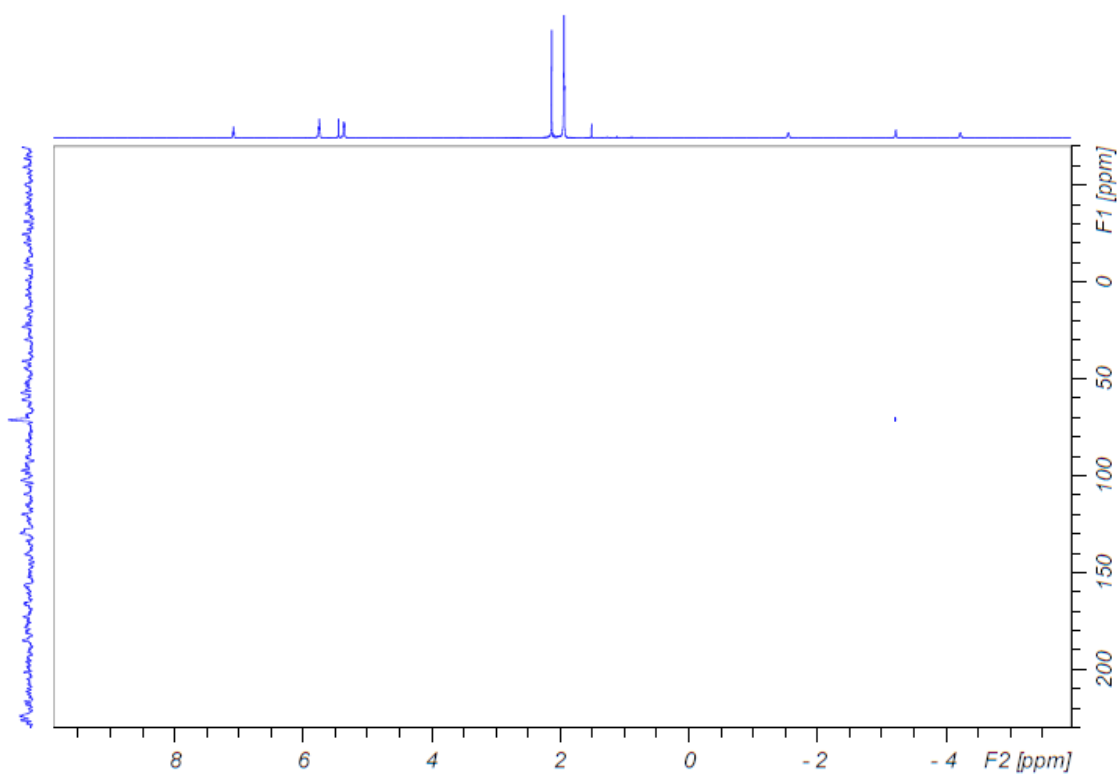**Figure S14:** ^{13}C-NMR spectrum of complex Fe(bppz)$_3$ in CD$_3$CN

Figure S15: ^{15}N-HMBC spectrum of Fe(bppz)$_3$ in CD$_3$CN

MeCN

TH-530-1-ESI-pos 1 (0.052)

1: TOF MS ES+
1.89e6
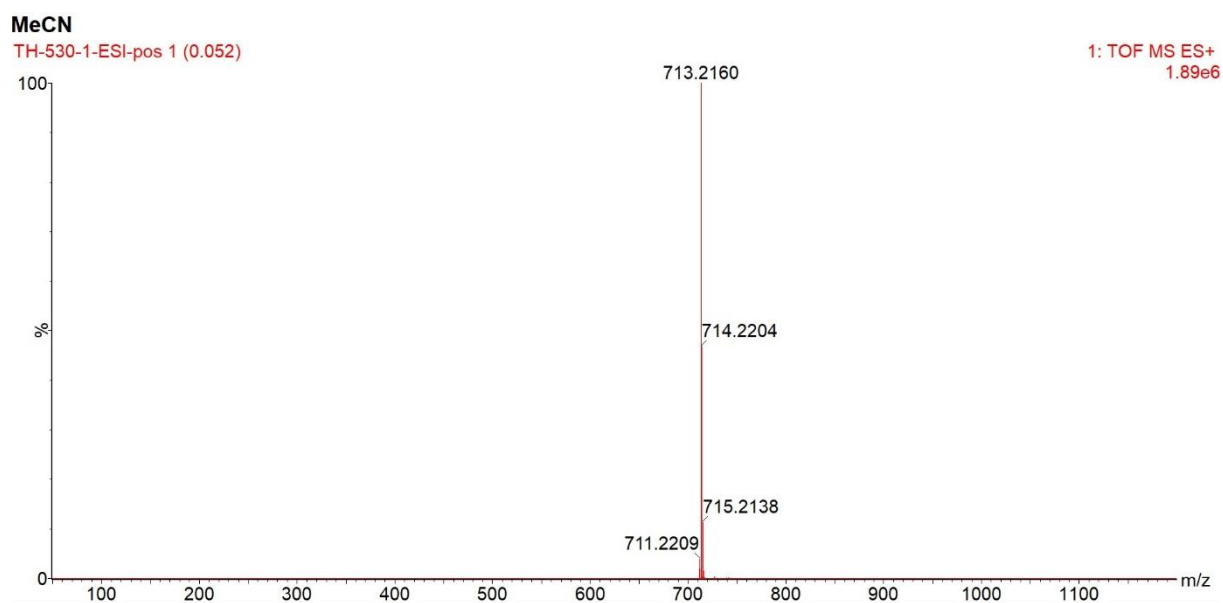
Figure S16: ESI-MS spectrum of complex Fe(bppz)$_3$ in CH$_3$CN
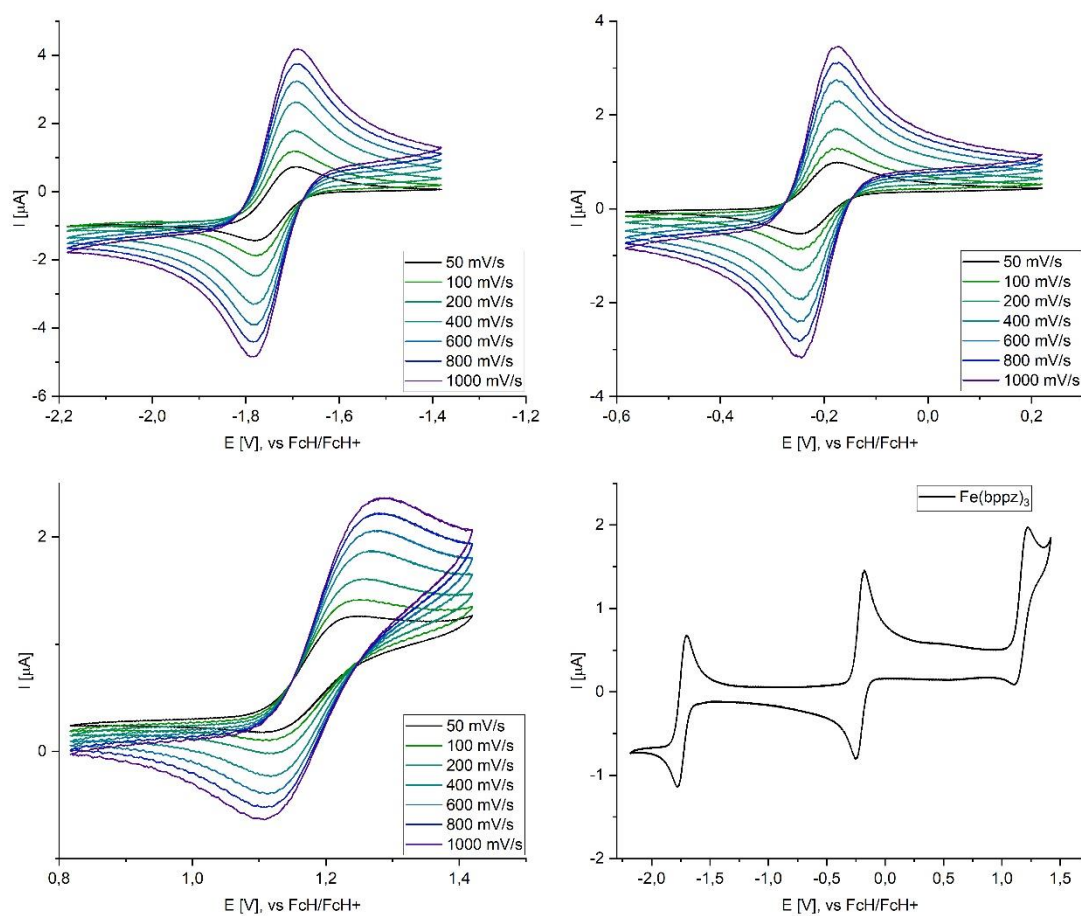
Figure S17: Cyclovoltammetry spectra of Fe(bppz)$_3$ in CH$_3$CN

Table S4: Cyclovoltammetry data for Fe(bppz)$_3$ at different scan rates, first redox step

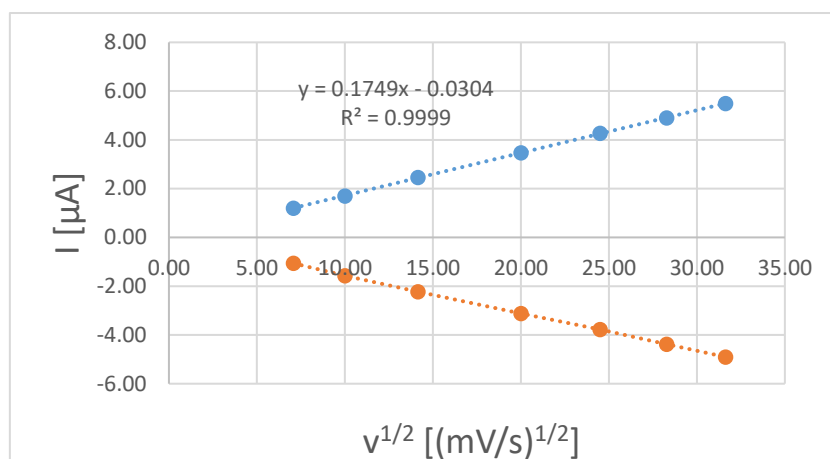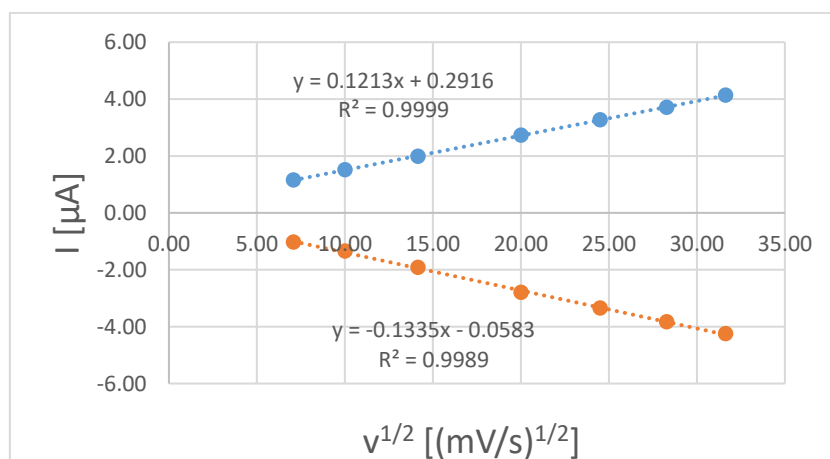| SCANRATE	[MV/S]	50	100	200	400	600	800	1000
E_{PC}	[V]	-1,774	-1,777	-1,772	-1,777	-1,777	-1,779	-1,777
E_{PA}	[V]	-1,699	-1,699	-1,696	-1,694	-1,699	-1,696	-1,696
$E_{1/2}$	[V]	-1,74	-1,74	-1,73	-1,74	-1,74	-1,74	-1,74
ΔE	[V]	0,076	0,078	0,076	0,083	0,078	0,083	0,081
I_{PC}	[µA]	-1,12	-1,58	-2,24	-3,10	-3,76	-4,27	-4,75
I_{PA}	[µA]	1,36	1,67	2,19	2,95	3,54	4,01	4,43
I_{PA}/I_{PC}		-1,21	-1,06	-0,98	-0,95	-0,94	-0,94	-0,93

Figure S18: Plotted data of Randles-Sevcik-Equation Fe(bppz)$_3$ at different scan rates, first redox step

Table S5: Cyclovoltammetry data for Fe(bppz)$_3$ at different scan rates, second redox step

| SCANRATE	[MV/S]	50	100	200	400	600	800	1000
E_{PC}	[V]	-0,241	-0,241	-0,246	-0,241	-0,241	-0,249	-0,244
E_{PA}	[V]	-0,175	-0,175	-0,180	-0,180	-0,175	-0,183	-0,173
$E_{1/2}$	[V]	-0,21	-0,21	-0,21	-0,21	-0,21	-0,22	-0,21
ΔE	[V]	0,066	0,066	0,066	0,061	0,066	0,066	0,071
I_{PC}	[µA]	-0,75	-1,09	-1,55	-2,18	-2,62	-3,04	-3,41
I_{PA}	[µA]	0,87	1,14	1,60	2,21	2,69	3,08	3,43
I_{PA}/I_{PC}		-1,17	-1,05	-1,04	-1,01	-1,03	-1,01	-1,01

Figure S19: Plotted data of Randles-Sevcik-Equation Fe(bppz)$_3$ at different scan rates, second redox step

Table S6: Cyclovoltammetry data for Fe(bppz)$_3$ at different scan rates, third redox step

SCANRATE	[MV/S]	50	100	200	400	600	800	1000
E_{PC}	[V]	1,129	1,127	1,134	1,132	1,124	1,122	1,110
E_{PA}	[V]	1,217	1,222	1,232	1,239	1,244	1,246	1,261
$E_{1/2}$	[V]	1,17	1,17	1,18	1,19	1,18	1,18	1,19
ΔE	[V]	0,088	0,095	0,098	0,107	0,120	0,125	0,151
I_{PC}	[µA]	-0,49	-0,58	-0,71	-0,95	-1,21	-1,33	-1,44
I_{PA}	[µA]	0,53	0,64	0,76	0,88	1,02	1,08	1,13
I_{PA}/I_{PC}		-1,08	-1,10	-1,07	-0,92	-0,84	-0,82	-0,78
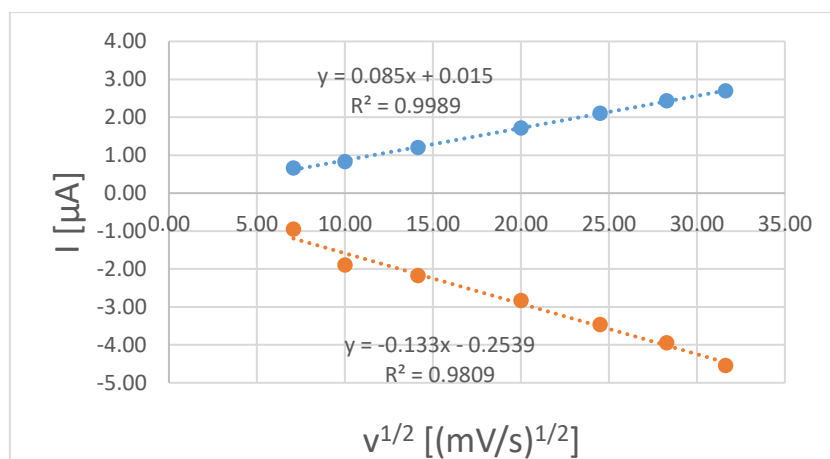
Figure S20: Plotted data of Randles-Sevcik-Equation Fe(bppz)$_3$ at different scan rates, third redox step
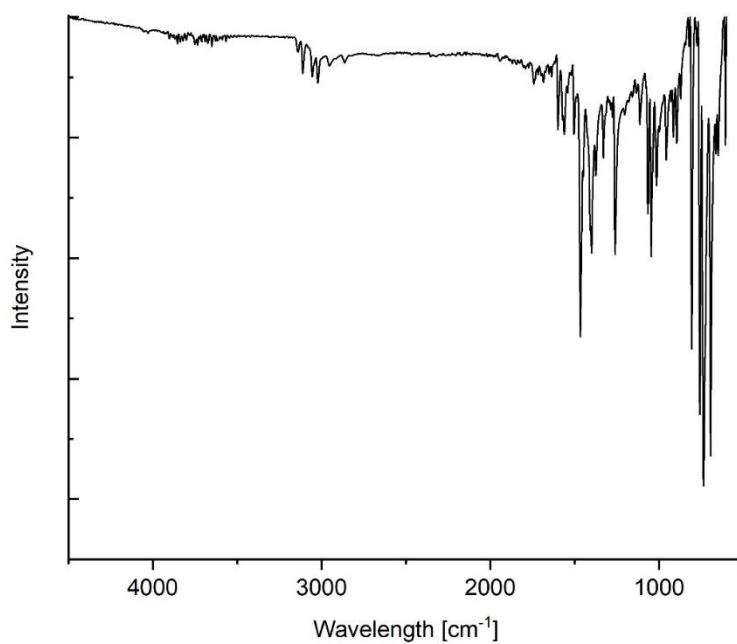
Figure S21: ATR-IR- spectrum of complex Fe(bppz)$_3$

Fe(CF$_3$ppz)$_3$

The complex was obtained as yellow powder (17.2%).

^{1}H-NMR (700.0 MHz, CD$_3$CN): δ = -75.17 (s, 1H, 2-*H*), -10.47 (s, 1H, 10-*H*), -3.39 (s, 1H, 9-*H*), -3.17 (s, 1H, 5-*H*), 0.27 (s, 1H, 6-*H*), 11.23 (s, 1H, 8-*H*) ppm.

^{13}C-NMR (176.1 MHz, CD$_3$CN): δ = -93.4 (1C, 3-*C*), -68.6 (1C, 6-*C*), 108.9 (1C, 8-*C*), 112.6 (1C, 9-*C*), 126.5 (1C, dd, $^1J_{CF}$ = 272.85 Hz 275.09 Hz, 4-*C*), 132.8 (1C, 10-*C*), 229.9 (1C, 5-*C*), 361.9 (1C, 2-*C*), 382.0 (1C, 7-*C*) ppm.

^{15}N-NMR (70.96 MHz, CD$_3$CN): 84.0 ppm.

^{19}F-NMR (659.0 MHz, CD$_3$CN): δ = -71.5 (s, 3F) ppm.

MS (ESI in MECN): m/z 689.0800 (for C$_{30}$H$_{18}$F$_9$FeN$_6$ calc. 689.0799).

Elemental analysis: calc. for C$_{30}$H$_{18}$F$_9$FeN$_6$: C: 52.27%, H: 2.63%, N: 12.19%, found: C: 51.90%, H: 2.81%, N: 12.12%.

IR (ATR, $\tilde{v}$ [cm^{-1}]): 3155w, 3033w, 2360w, 2335w, 1585w, 1508w, 1477w, 1396m, 1315s, 1272s, 1249m, 1159m, 1110s, 1066s, 1045s, 960m, 900m, 838w, 821w, 804m, 746s, 702m, 661m, 607w.
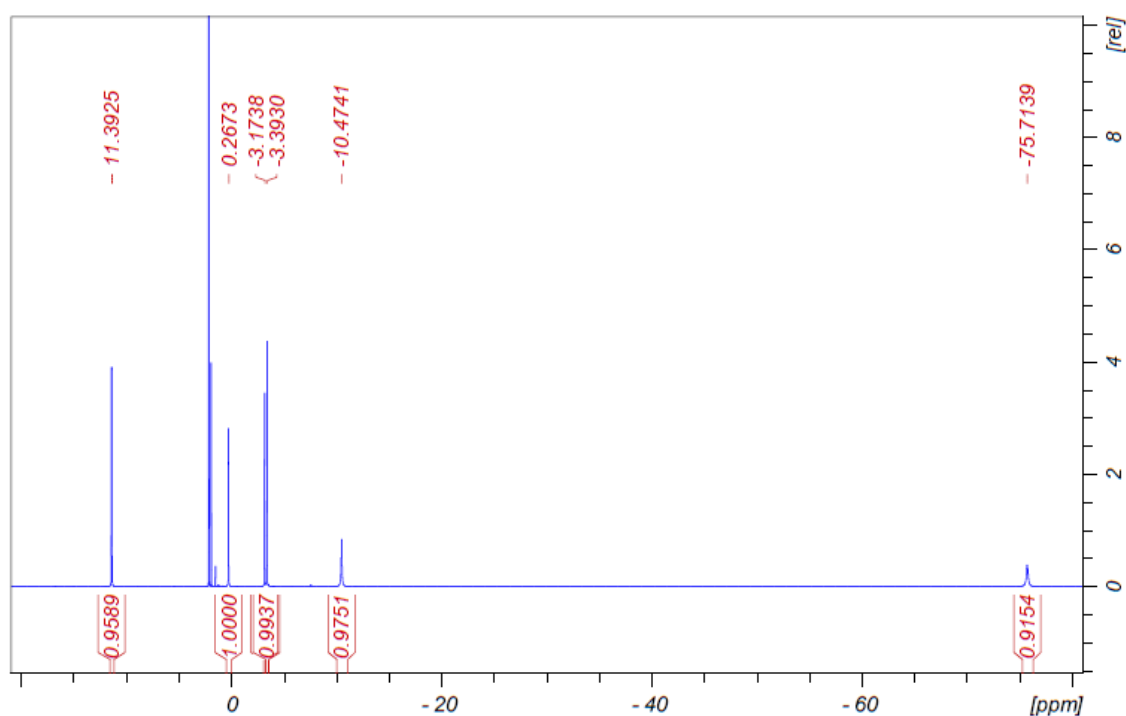
Figure S22:^{1}H-NMR spectra of complex Fe(CF$_3$ppz)$_3$ in CD$_3$CN
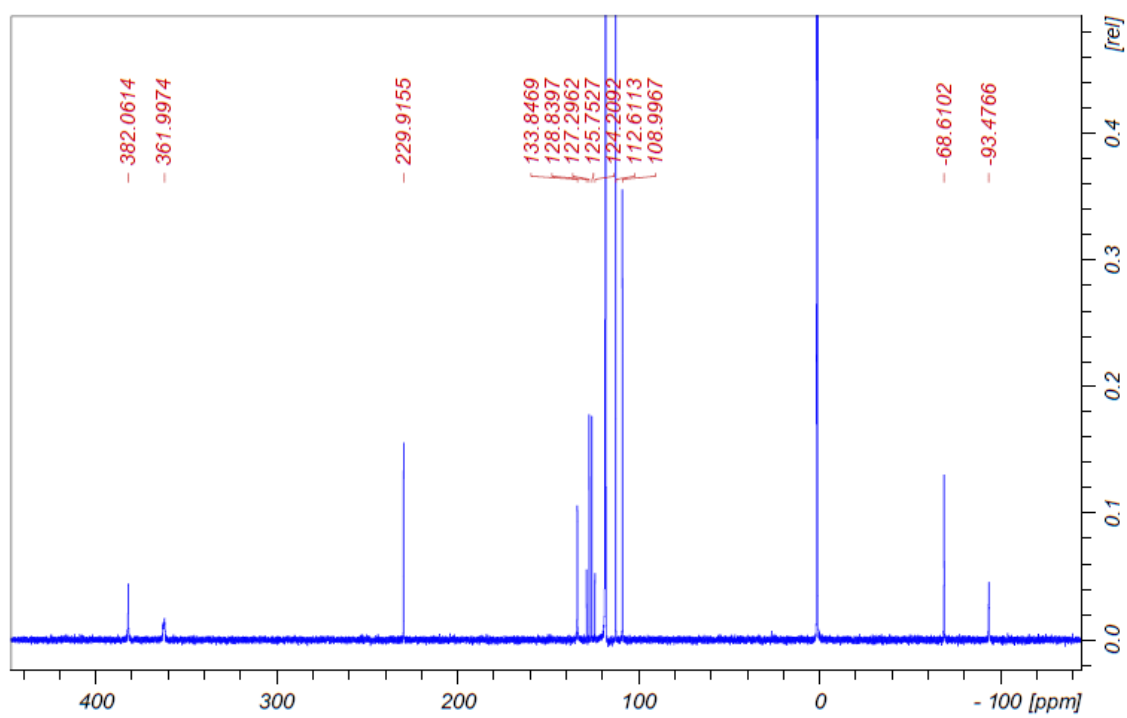
Figure S23: ^{13}C-NMR spectra of complex Fe(CF$_3$ppz)$_3$ in CD$_3$CN
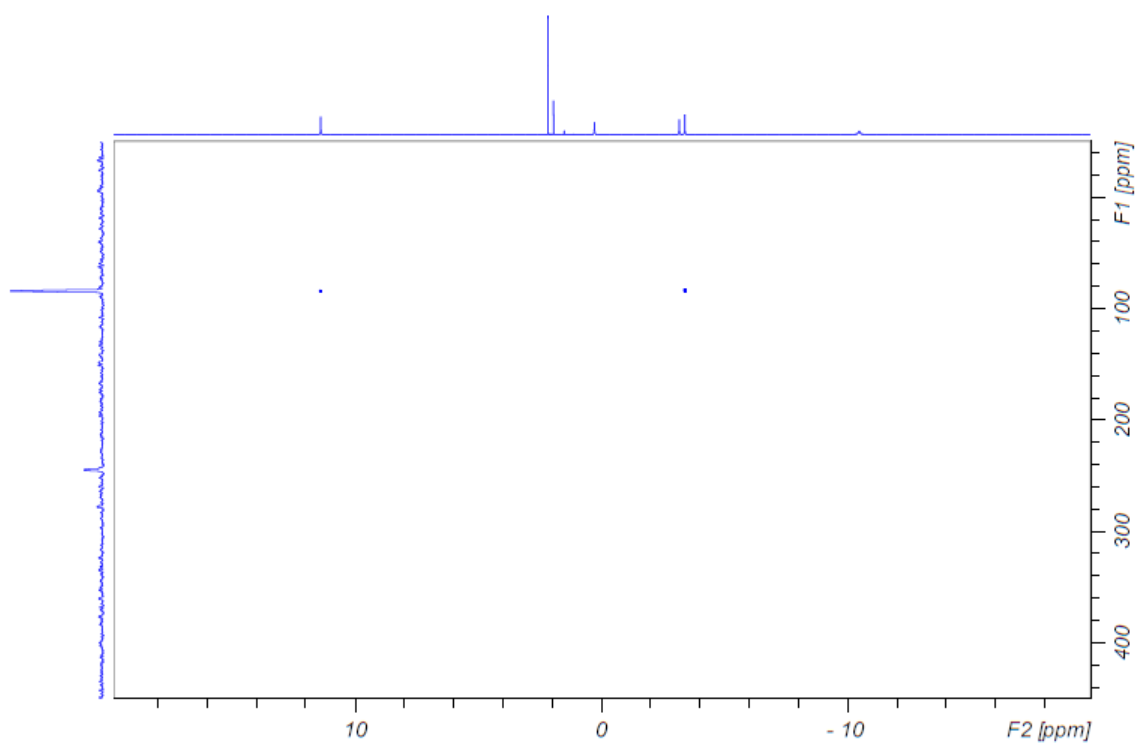
Figure S24: ^{15}N-HMBC spectrum of the complex Fe(CF$_3$ppz)$_3$ in CD$_3$CN
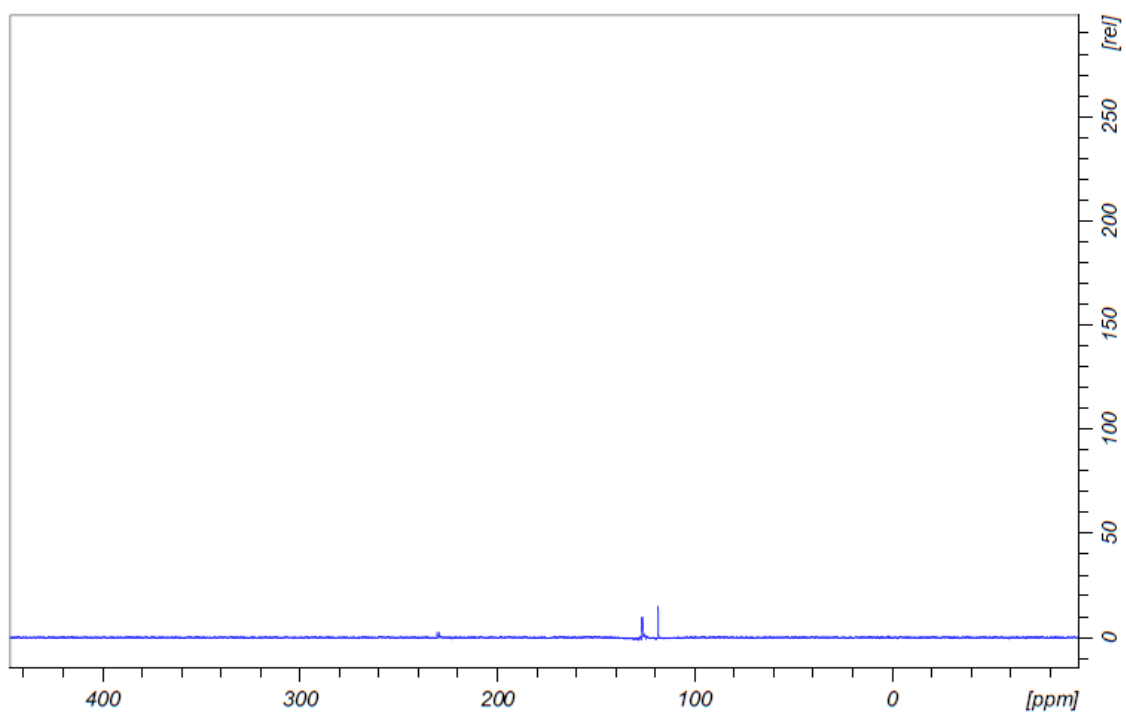
Figure S25:^{19}F-HMBC spectrum of the complex Fe(CF$_3$ppz)$_3$ in CD$_3$CN
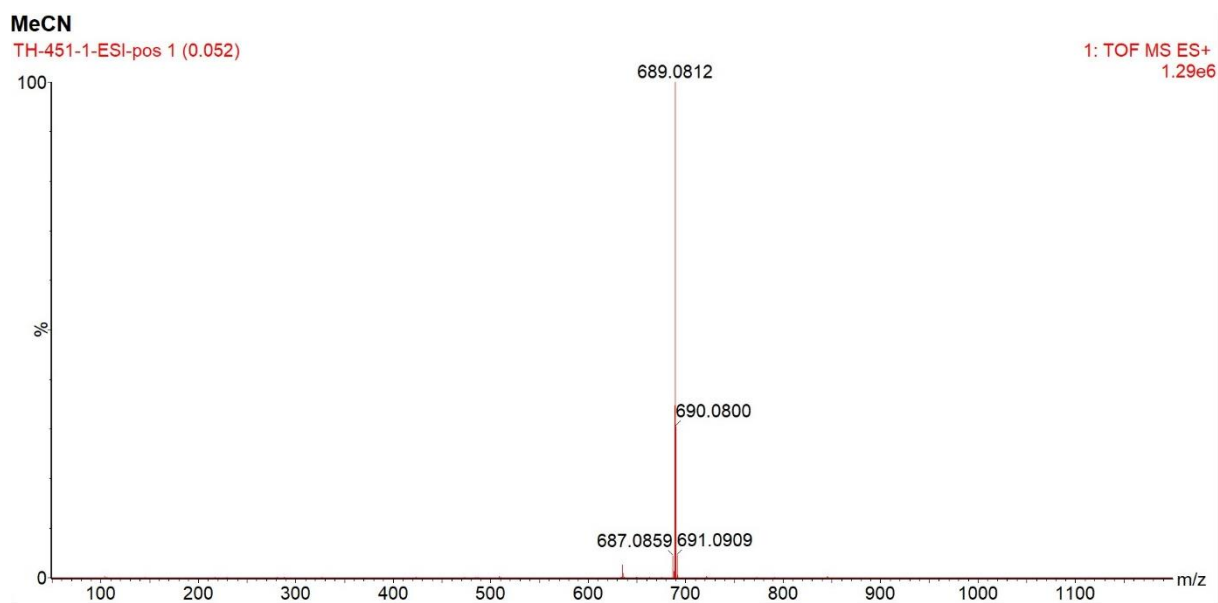
Figure S26: ESI-MS of complex Fe(CF$_3$ppz)$_3$ in CH$_3$CN

17
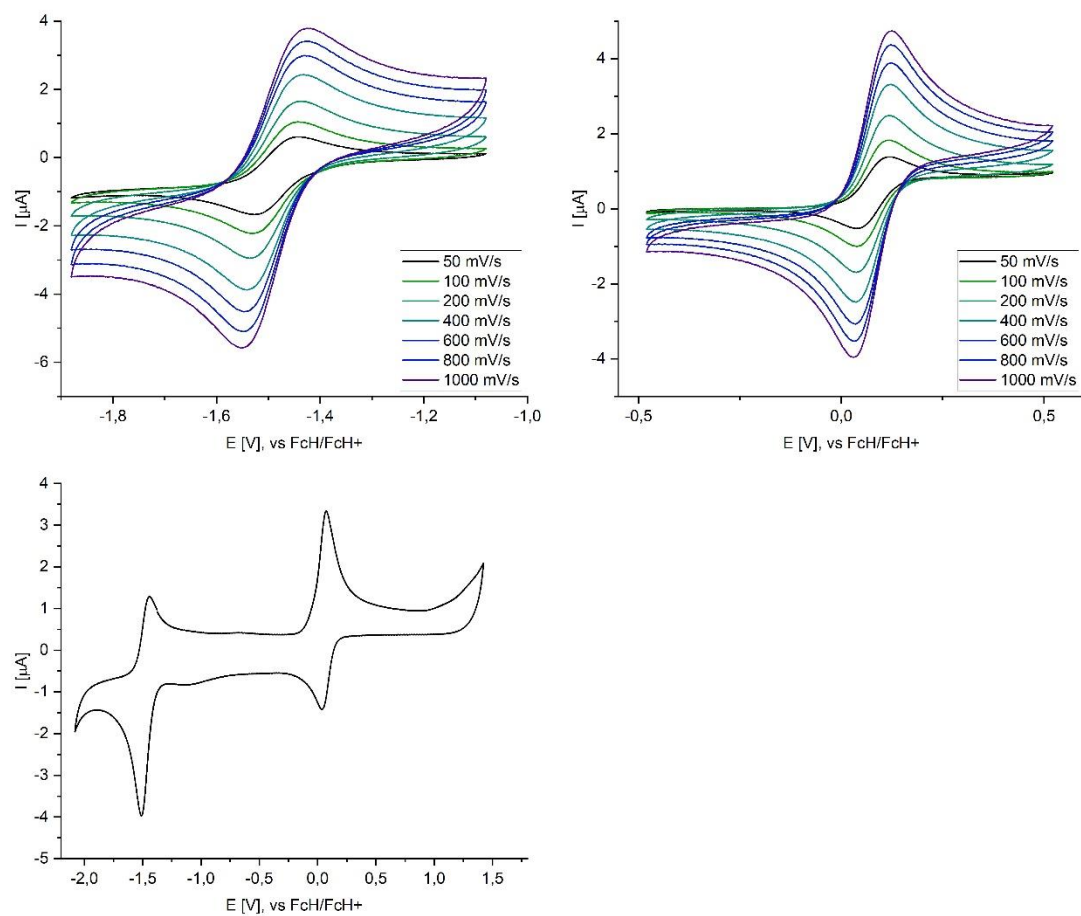
Figure S27: Cyclovoltammetry spectra of Fe(CF$_3$ppz)$_3$ in CH$_3$CN

Table S7: Cyclovoltammetry data for Fe(CF$_3$ppz)$_3$ at different scan rates, first redox step

SCANRATE	[MV/S]	50	100	200	400	600	800	1000
E$_{PC}$	[V]	-1,522	-1,524	-1,531	-1,539	-1,541	-1,544	-1,541
E$_{PA}$	[V]	-1,448	-1,443	-1,441	-1,439	-1,436	-1,439	-1,434
E$_{1/2}$	[V]	-1,48	-1,48	-1,49	-1,49	-1,49	-1,49	-1,49
ΔE	[V]	0,073	0,081	0,090	0,100	0,105	0,105	0,107
I$_{PC}$	[µA]	-1,13	-1,59	-2,25	-2,99	-3,50	-3,95	-4,24
I$_{PA}$	[µA]	1,10	1,48	2,02	2,63	3,03	3,35	3,63
I$_{PA}$/I$_{PC}$		-0,97	-0,93	-0,90	-0,88	-0,86	-0,85	-0,86
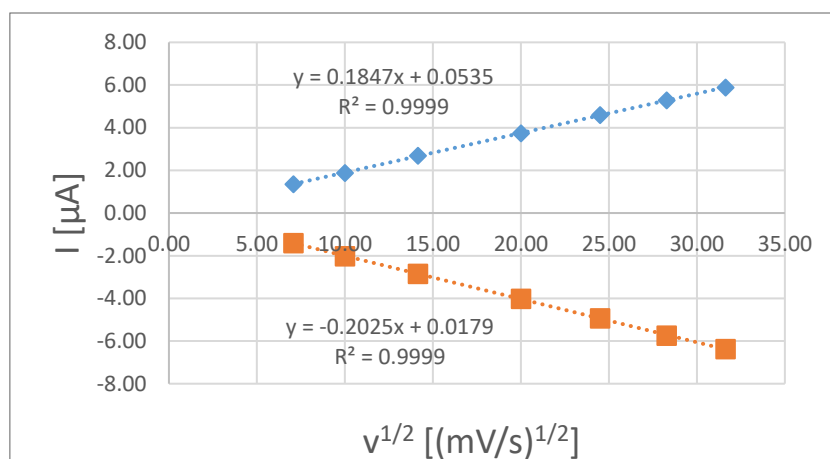
Figure S28: Plotted data of Randles-Sevcik-Equation Fe(CF$_3$ppz)$_3$ at different scan rates, first redox step

Table S8: Cyclovoltammetry data for Fe(CF$_3$ppz)$_3$ at different scan rates, second redox step

SCANRATE	[MV/S]	50	100	200	400	600	800	1000
E_{PC}	[V]	0,045	0,040	0,037	0,037	0,035	0,037	0,033
E_{PA}	[V]	0,113	0,113	0,118	0,120	0,123	0,118	0,118
$E_{1/2}$	[V]	0,08	0,08	0,08	0,08	0,08	0,08	0,08
ΔE	[V]	0,068	0,073	0,081	0,083	0,088	0,081	0,085
I_{PC}	[µA]	-1,11	-1,55	-2,22	-3,02	-3,63	-4,11	-4,54
I_{PA}	[µA]	1,03	1,47	2,04	2,79	3,33	3,77	4,13
I_{PA}/I_{PC}		-0,93	-0,95	-0,92	-0,92	-0,92	-0,92	-0,91
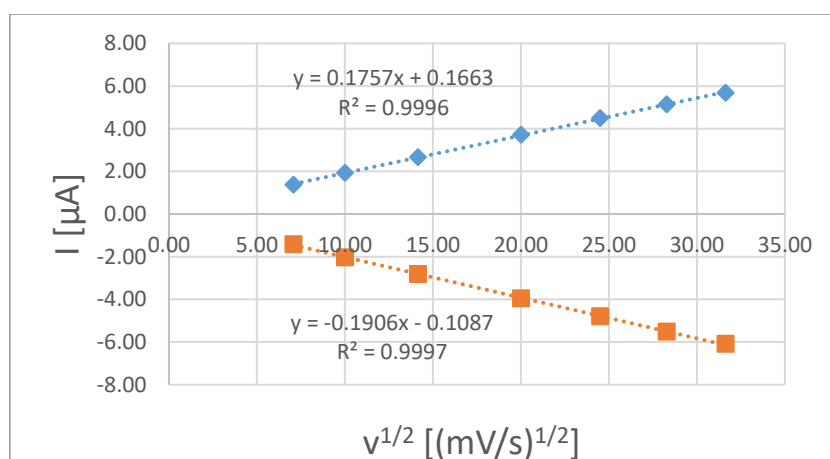
Figure 29: Plotted data of Randles-Sevcik-Equation Fe(CF$_3$ppz)$_3$ at different scan rates, first redox step
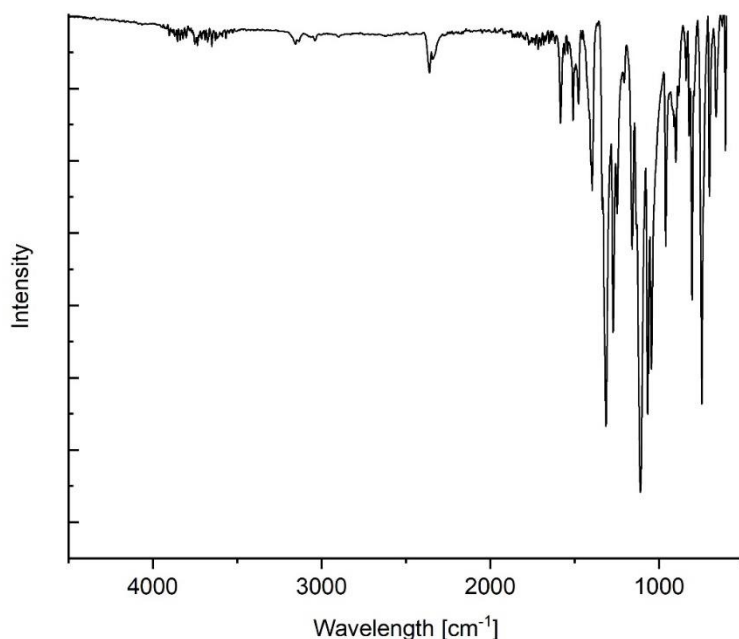
Figure S30: ATR-IR-spectrum of complex Fe(CF$_3$ppz)$_3$

Fe(naphpz)$_3$

The complex was obtained as red powder (5.3%).

^{1}H-NMR (700 MHz, DMSO-d6): δ = -85.19 (s, 1H, 2-*H*), -12.51 (s, 1H, 13-*H*), -1.68 (d, $^3J_{HH}$ = 6.3 Hz, 1H, 4-*H*), -1.31 (s, 1H, 12-*H*), 1.10 (s, 1H, 9-*H*), 1.25 (t, $^3J_{HH}$ = 7.10 Hz, 1H, 6-*H*), 8.12 (t, $^3J_{HH}$ = 6.30 Hz, 1H, 5-*H*), 11.15 (s, 1H, 11-*H*), 12.83 (d, $^3J_{HH}$ = 8.50 Hz, 1H, 7-*H*) ppm.

^{13}C-NMR* (176.1 MHz, DMSO-d6): δ = -97.6 (1C, 3-*C*), -56.79 (1C, 150.66 Hz, 9-*C*), 80.3 (1C, 150.66 Hz, 7-*C*), 81.6 (1C, 160.34 Hz, 5-*C*), 99.4 (1C, 180.91 Hz, 12-*C*), 124.3 (2C, 188.74 Hz, 11-*C*), 126.6 (1C, 188.74 Hz, 13-*C*), 172.1 (2C, 157.98 Hz, 6-*C*), 180.5 (1C, 157.98 Hz, 4-*C*), 216.3 (1C, 8-*C*), 365.3 (1C, 2-*C*), 413.9 (1C, 10-*C*) ppm.

MS (ESI in MECN): m/z 635.1640 (for C$_{39}$H$_{27}$FeN$_6$ calc. 635.1647).

Elemental analysis: calc. for C$_{39}$H$_{27}$FeN$_6$: C: 73.71%, H: 4.28%, N: 13.22%, found: C: 74.29%, H: 5.10%, N: 12.42%. **IR** (ATR, $\tilde{v}$ [cm^{-1}]): 3126w, 6047w, 2917w, 2854w, 1585w, 1593w, 1560w, 1510w, 1486w,

1459m, 1405m, 1332w, 1313w, 1251w, 1197w, 1134w, 1107w, 1062m, 1037w, 977w, 935w, 889w, 856m, 831w, 736s, 682w, 651w.
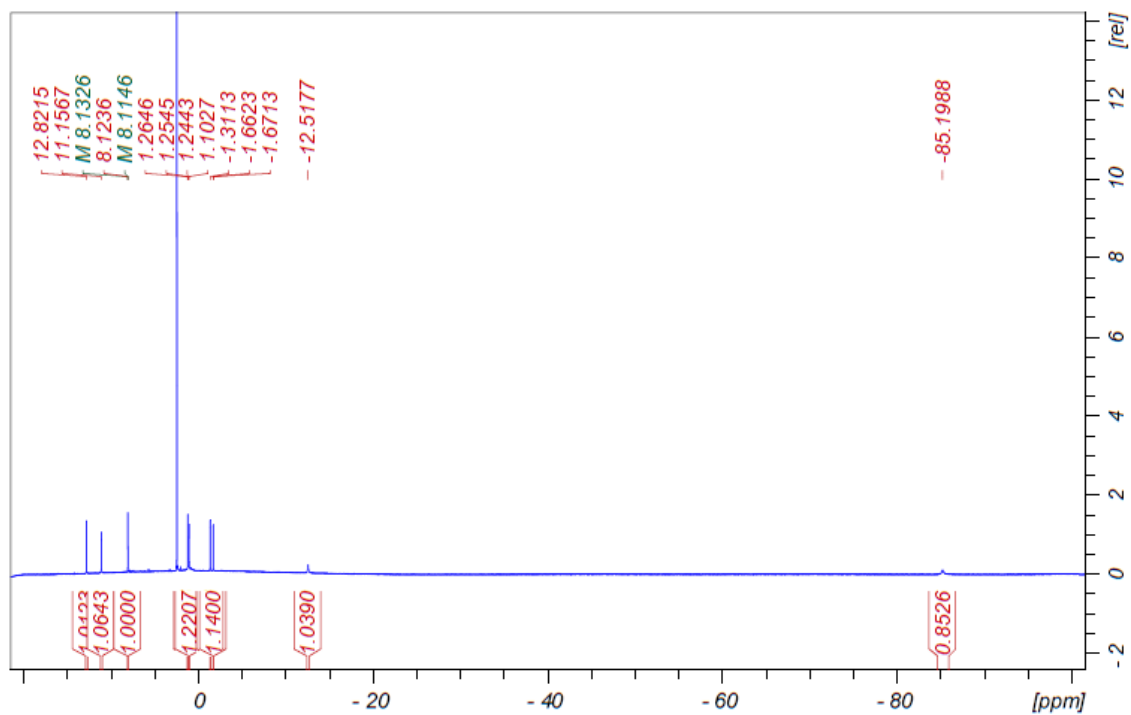
*not decoupled

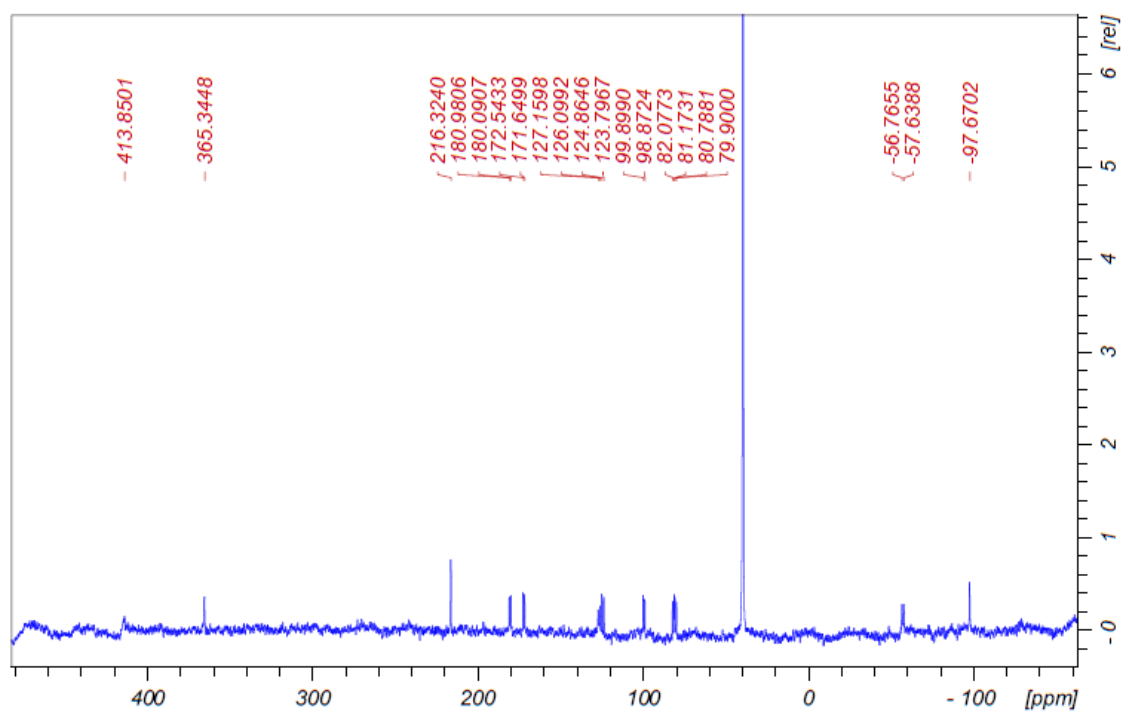**Figure S31**: ^{1}H-NMR spectrum of complex Fe(naphpz)$_3$ in DMSO-d^6

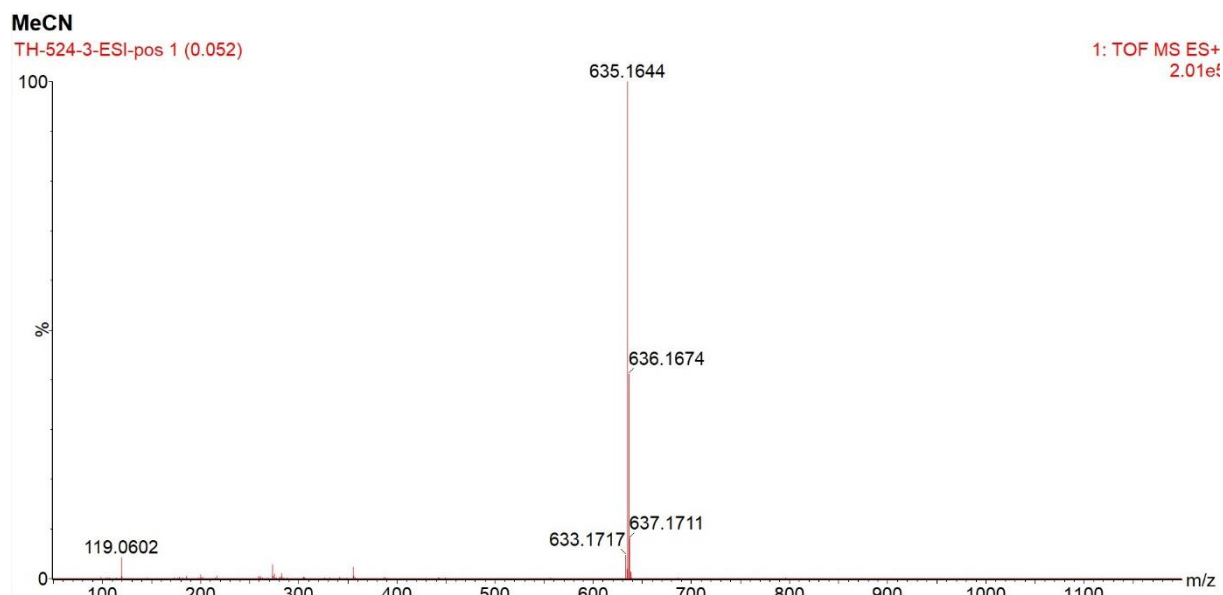**Figure S32:** ^{13}C-NMR spectrum of complex Fe(naphpz)$_3$ in DMSO-d^6

TH-524-3-ESI-pos 1 (0.052)

1: TOF MS ES+
2.01e5

635.1644

636.1674

119.0602

633.1717 637.1711

Figure S33: ESI-MS spectrum of complex Fe(naphpz)$_3$ in CH$_3$CN
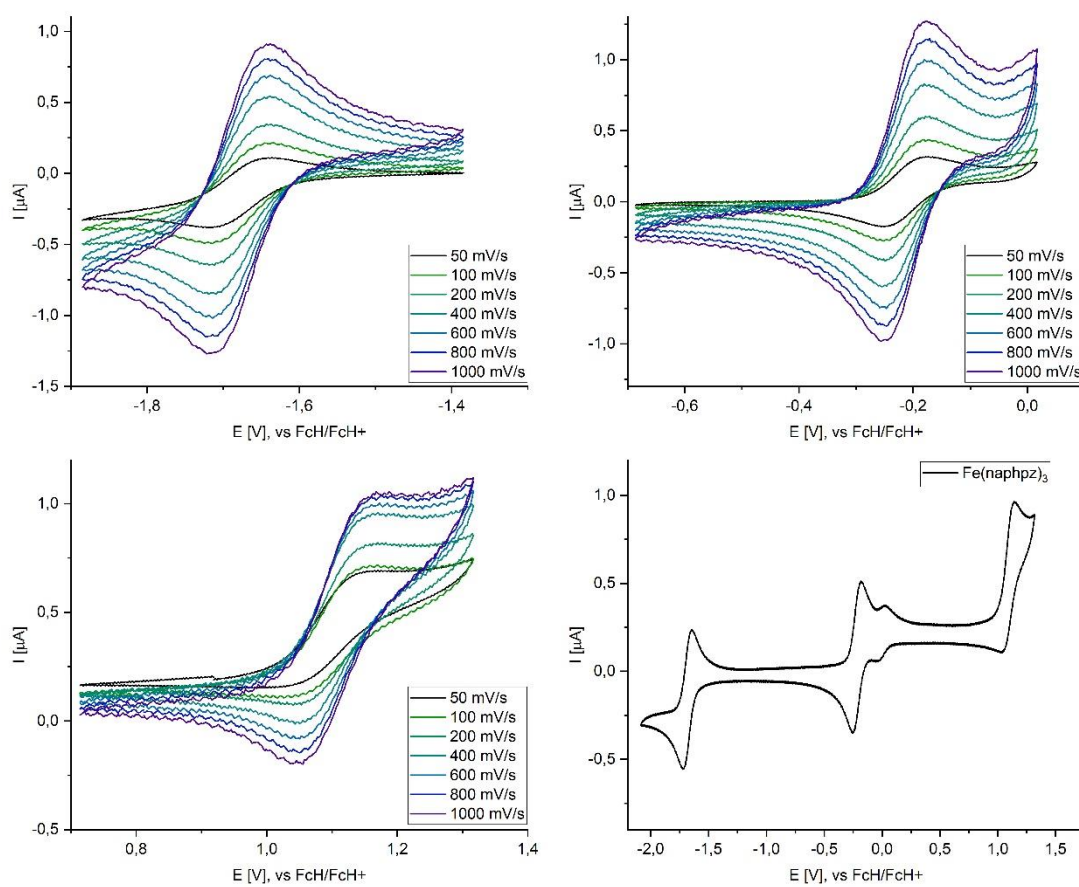
Figure S34: Cyclovoltammetry spectra of complex Fe(naphpz)$_3$ in CH$_3$CN

Table S9: Cyclovoltammetry data for Fe(naphpz)$_3$ at different scan rates, first redox step

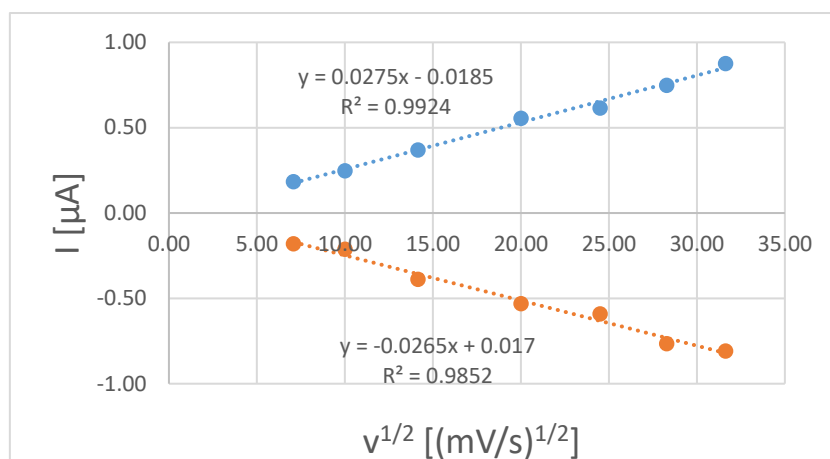| SCANRATE	[MV/S]	50	100	200	400	600	800	1000
E_{PC}	[V]	-1,712	-1,712	-1,712	-1,717	-1,714	-1,709	-1,714
E_{PA}	[V]	-1,638	-1,641	-1,648	-1,643	-1,648	-1,648	-1,643
$E_{1/2}$	[V]	-1,68	-1,68	-1,68	-1,68	-1,68	-1,68	-1,68
ΔE	[V]	0,073	0,071	0,064	0,073	0,066	0,061	0,071
I_{PC}	[µA]	-0,18	-0,21	-0,39	-0,53	-0,59	-0,77	-0,81
I_{PA}	[µA]	0,18	0,25	0,37	0,56	0,62	0,75	0,88
I_{PA}/I_{PC}		-1,02	-1,18	-0,95	-1,05	-1,04	-0,98	-1,08
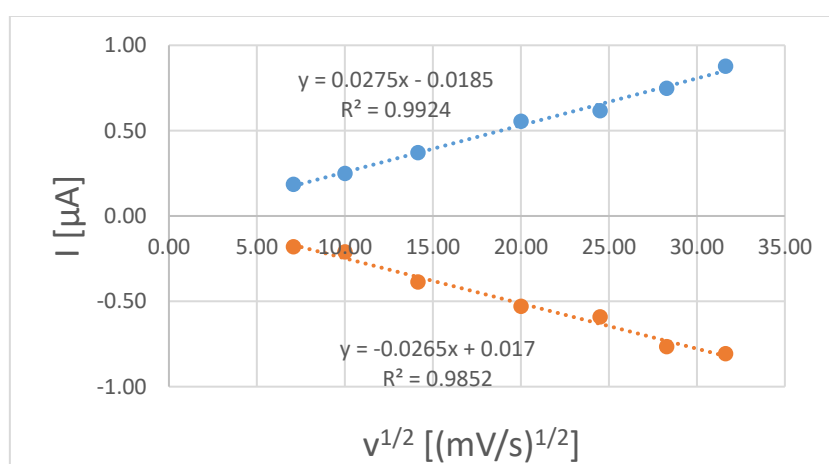
Figure S35: Plotted data of Randles-Sevcik-Equation Fe(naphpz)$_3$ at different scan rates, first redox step

Table S10: Cyclovoltammetry data for Fe(naphpz)$_3$ at different scan rates, second redox step

SCANRATE	[MV/S]	50	100	200	400	600	800	1000
E_{PC}	[V]	-0,248	-0,251	-0,246	-0,251	-0,257	-0,243	-0,253
E_{PA}	[V]	-0,177	-0,182	-0,182	-0,192	-0,191	-0,190	-0,185
$E_{1/2}$	[V]	-0,21	-0,22	-0,21	-0,22	-0,22	-0,22	-0,22
ΔE	[V]	0,071	0,068	0,063	0,059	0,066	0,054	0,068
I_{PC}	[µA]	-0,15	-0,22	-0,35	-0,65	-0,83	-0,71	-0,79
I_{PA}	[µA]	0,17	0,19	0,32	0,52	0,65	0,55	0,60
I_{PA}/I_{PC}		-1,10	-0,86	-0,91	-0,80	-0,79	-0,76	-0,76

Figure S36: Plotted data of Randles-Sevcik-Equation Fe(naphpz)$_3$ at different scan rates, second redox step

Table S11: Cyclovoltammetry data for Fe(naphpz)$_3$ at different scan rates, second redox step

SCANRATE	[MV/S]	50	100	200	400	600	800	1000
E_{PC}	[V]	1,037	1,035	1,057	1,049	1,057	1,059	1,062
E_{PA}	[V]	1,125	1,130	1,127	1,140	1,130	1,127	1,125
$E_{1/2}$	[V]	1,08	1,08	1,09	1,09	1,09	1,09	1,09
ΔE	[V]	0,088	0,095	0,071	0,090	0,073	0,068	0,063
I_{PC}	[µA]	-0,18	-0,30	-0,37	-0,44	-0,51	-0,54	-0,61
I_{PA}	[µA]	0,20	0,25	0,35	0,43	0,46	0,50	0,52
I_{PA}/I_{PC}		-1,07	-0,84	-0,94	-0,98	-0,90	-0,92	-0,86
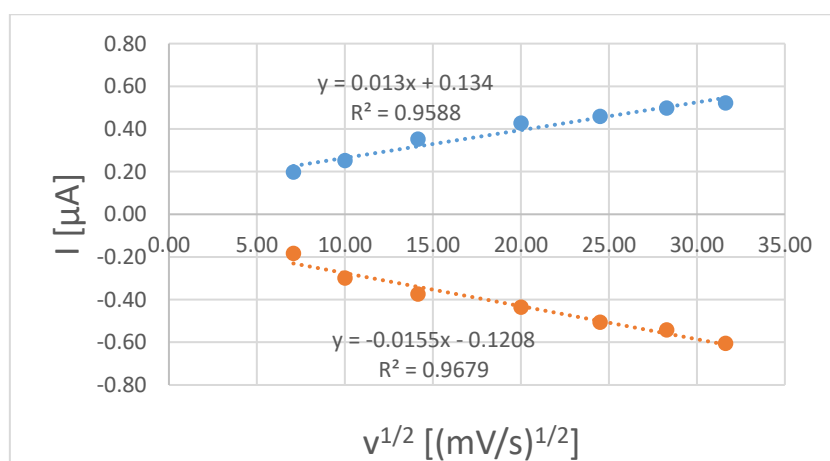
Figure S37: Plotted data of Randles-Sevcik-Equation Fe(naphpz)$_3$ at different scan rates, first redox step
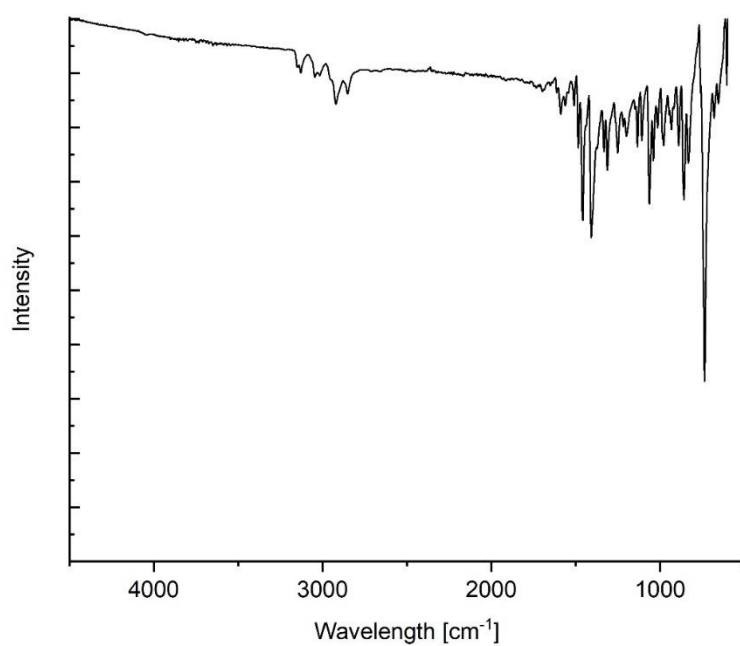
Figure S38: ATR-IR-spectrum of complex Fe(naphpz)$_3$ in CH$_3$CN
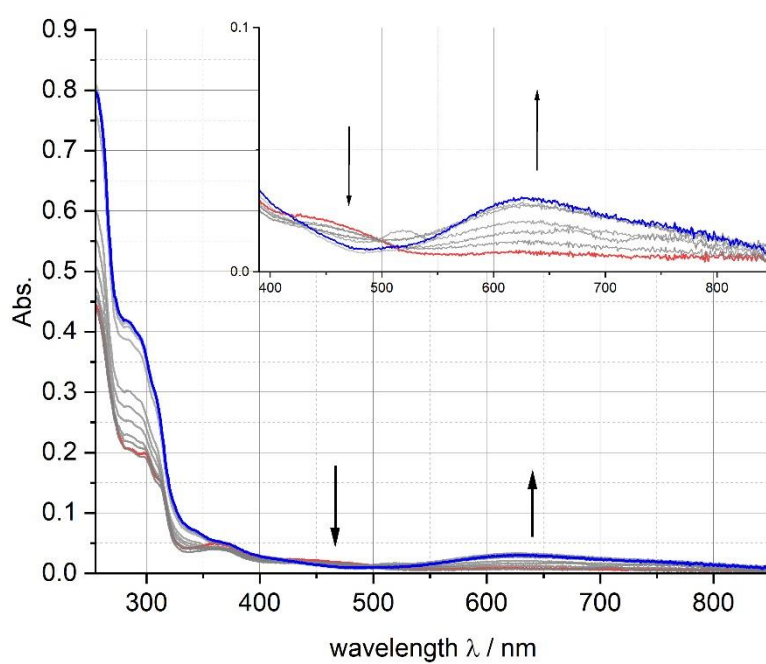
Figure S39: Change in the absorptive behaviour of (Fe(naphpz)$_3$ with an applied potential of 0.8-2 V in CH$_3$CN
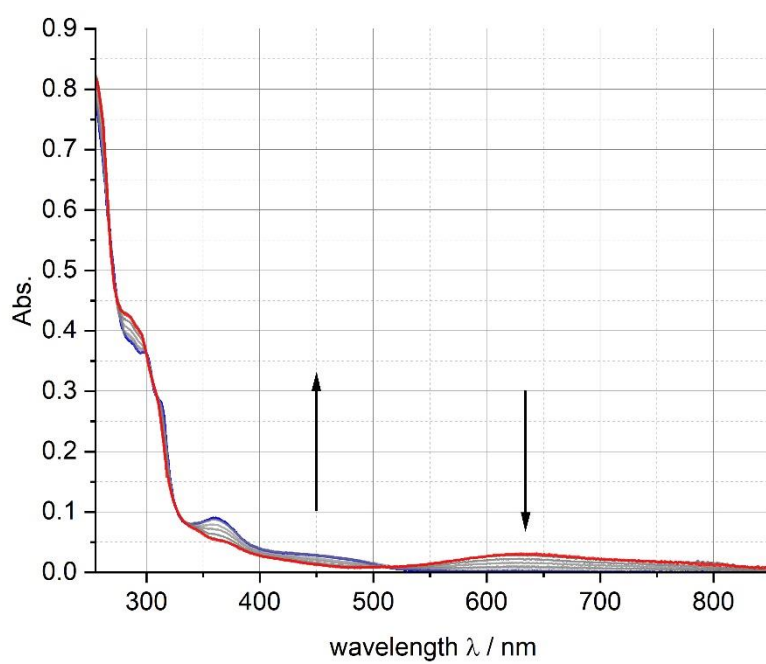
Figure S40: Change in the absorptive behaviour of (Fe(naphpz)$_3$ with an applied potential of -0.5-(-1.5) V in CH$_3$CN
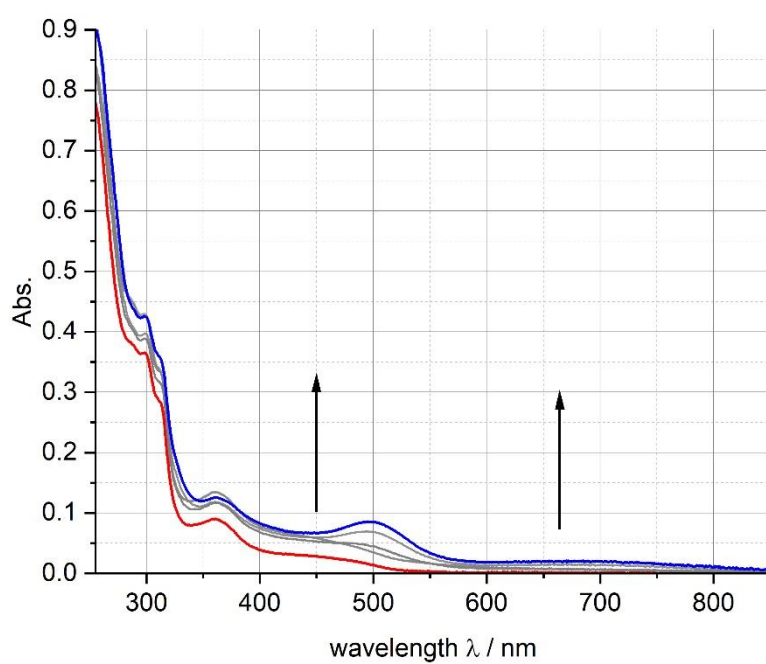
Figure S41: Change in the absorptive behaviour of (Fe(naphpz)$_3$ with an applied potential of -2.5 V in CH$_3$CN

<u>Fe(MeOppz)$_3$</u>

The complex was obtained as red powder (2.6%).

^{1}H-NMR (700 MHz, CD$_3$CN): δ = -79.93 (s, 1H, 2-*H*), -10.34 (s, 1H, 10-*H*), -5.36 (s, 1H, 6-*H*)), -5.12 (s, 1H, 5-*H*), -3.19 (s, 1H, 9-*H*), 1.44 (s, 3H, 4-*H*), 12.06 (s, 1H, 8-*H*) ppm.

^{13}C-NMR* (176.1 MHz, CD$_3$CN): δ = -106.1 (1C, 156.6 Hz, 6-*C*), -93.0 (1C, 3-*C*), 49.1 (1C, 139.07 Hz, 4-*C*), 103.9 (1C, 182.9 Hz, 8-*C*), 114.1 (1C, 191.7 Hz, 9-*C*) 130.1 (1C, 182.9 Hz, 10-*C*), 232.4 (1C, 159.9 Hz, 5-*C*), 360.8 (1C, 129.6 Hz, 2-*C*), 403.2 (1C, 7-*C*) ppm.

^{15}N-NMR (70.96 MHz, CD$_3$CN): 80.2 ppm.

MS (ESI in MECN): m/z 575.1530 (for C$_{30}$H$_{27}$FeN$_6$O$_3$ calc. 575.1494).

Elemental analysis: calc. for C$_{30}$H$_{27}$FeN$_6$O$_3$: C: 62.62%, H: 4.73%, N: 14.61%, found: C:62.49%, H: 5.19%, N: 14.35%.

IR (ATR, $\tilde{\upsilon}$ [cm^{-1}]): 3122w, 3039w, 3006w, 2952w, 2931w, 2902w, 2829w, 1583w, 1560s, 1506w, 1469s, 1417s, 1315m, 1276s, 1249m, 1209s, 1174s, 1116m, 1031s, 958m, 879m, 811w, 784s, 744s, 661w, 621m, 609m.

*not decoupled
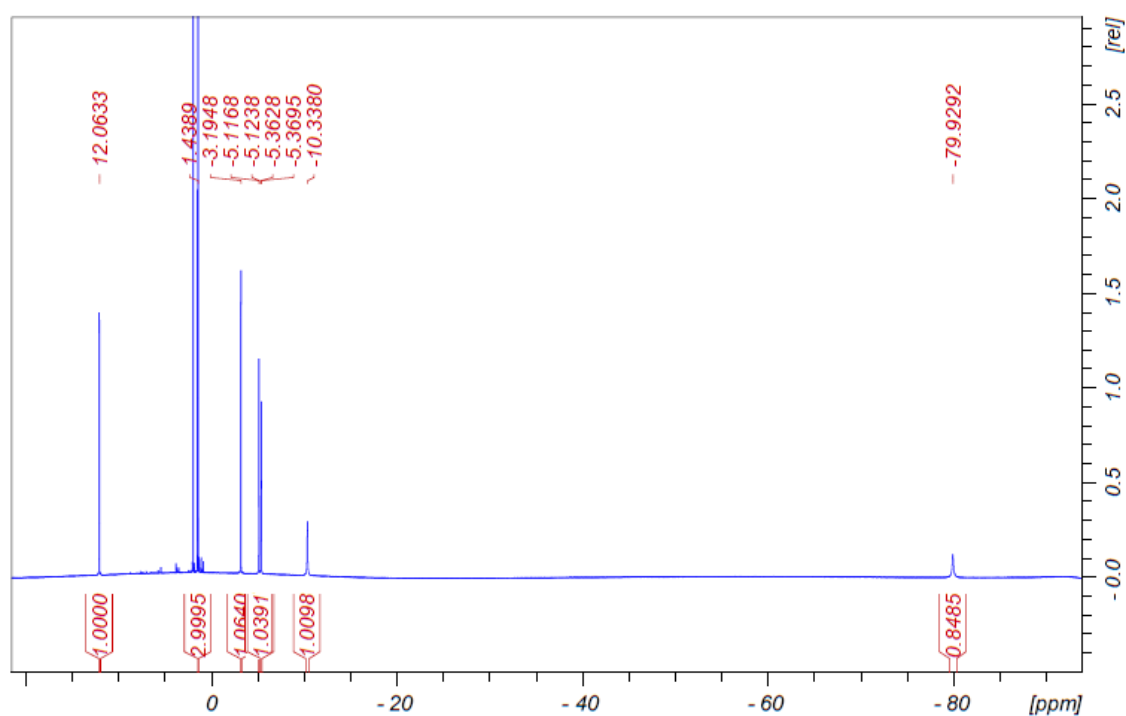
Figure S42: ^{1}H-NMR spectrum of complex Fe(MeOppz)$_3$ in CD$_3$CN
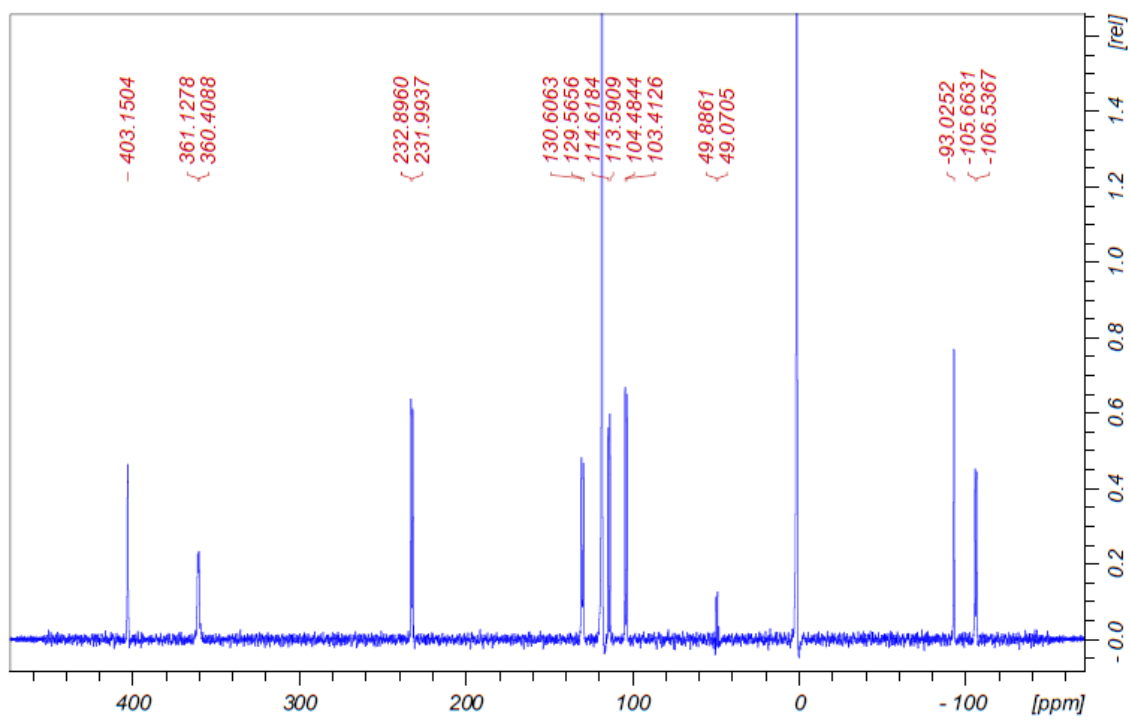
Figure S43: ^{13}C-NMR spectrum of complex Fe(MeOppz)$_3$ in CD$_3$CN

Peak labels (left to right):
403.1504
361.1278
360.4088
232.8960
231.9937
130.6063
129.5656
114.6184
113.5909
104.4844
103.4126
49.8861
49.0705
-93.0252
-105.6631
-106.5367
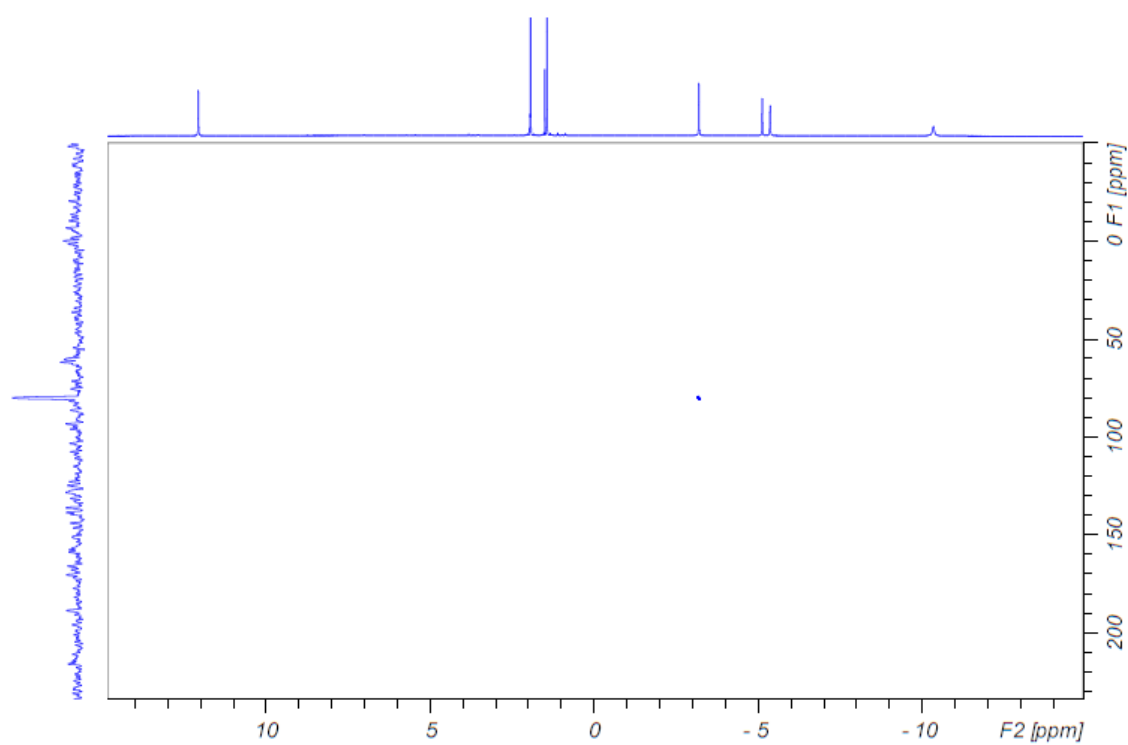
Figure S44: ^{15}N-HMBC spectrum of Fe(MeOppz)$_3$ in CD$_3$CN

28

MeCN

1: TOF MS ES+
8.08e5

575.1523

576.1487

573.1516 577.1566

100

%

0

100 200 300 400 500 600 700 800 900 1000 1100

m/z
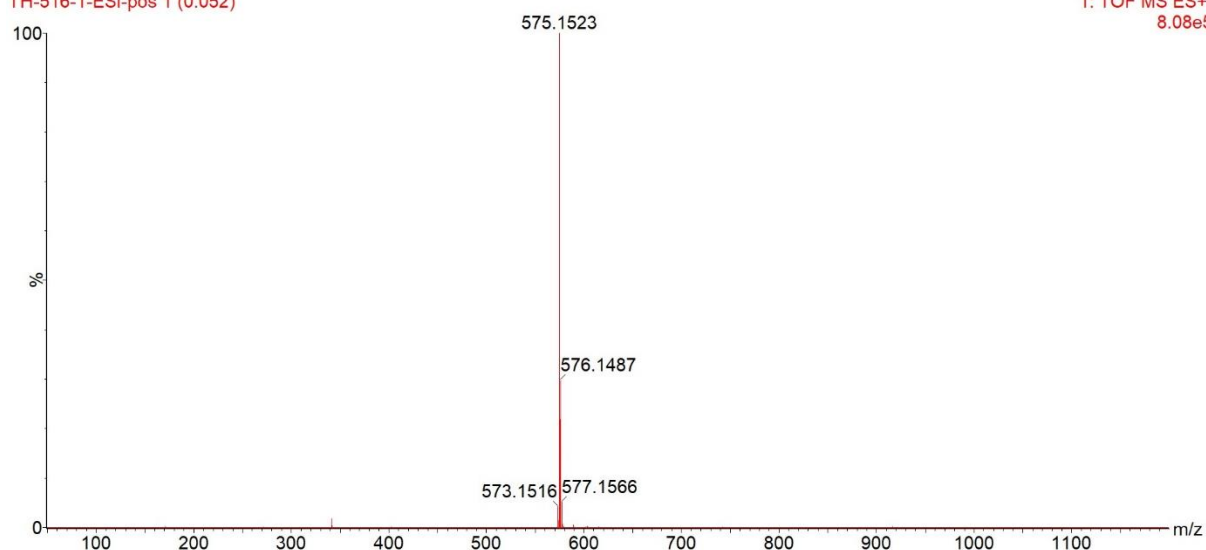
Figure S45: ESI-MS spectrum of complex Fe(MeOppz)$_3$ in CH$_3$CN
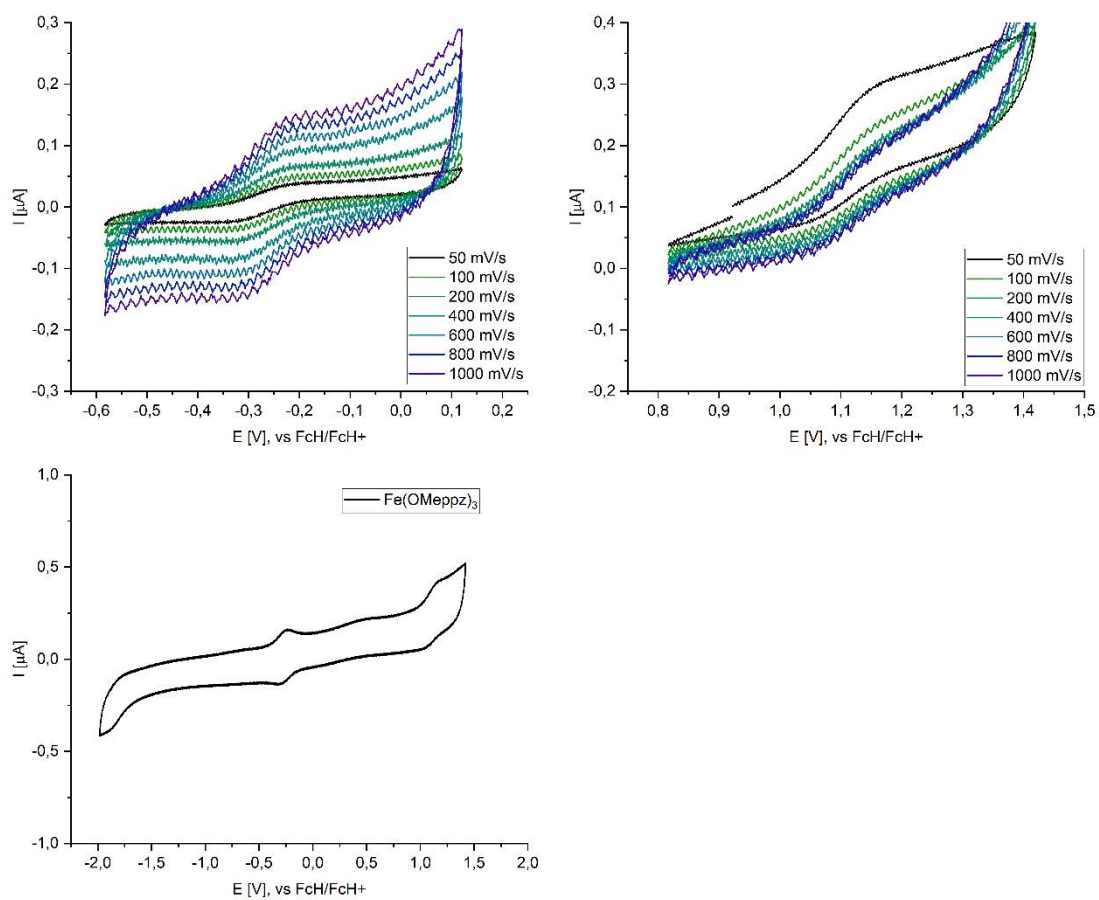
Figure S46: Cyclovoltammetry spectra of complex Fe(MeOppz)$_3$ in CH$_3$CN

29

Table S12: Cyclovoltammetry data for Fe(MeOppz)$_3$ at different scan rates, first redox step

SCANRATE	[MV/S]	50	100	200	400	600	800	1000
E_{PC}	[V]	-1,746	-1,753	-1,751	-1,748	-1,751	-1,748	-1,751
E_{PA}	[V]	-1,814	-1,812	-1,814	-1,812	-1,817	-1,814	-1,819
$E_{1/2}$	[V]	-1,78	-1,78	-1,78	-1,78	-1,78	-1,78	-1,78
ΔE	[V]	-0,068	-0,059	-0,063	-0,063	-0,066	-0,066	-0,068
I_{PC}	[µA]	-1,18	-1,61	-2,34	-3,35	-4,11	-4,71	-5,33
I_{PA}	[µA]	1,27	1,80	2,52	3,59	4,37	5,03	5,57
I_{PA}/I_{PC}		-1,08	-1,12	-1,08	-1,07	-1,06	-1,07	-1,04

Plot with:
$y = 0.176x + 0.0388$
$R^2 = 0.9998$

$y = -0.1698x + 0.0578$
$R^2 = 0.9997$

Axis labels: $I\ [\mu A]$ (vertical), $v^{1/2}\ [(mV/s)^{1/2}]$ (horizontal)
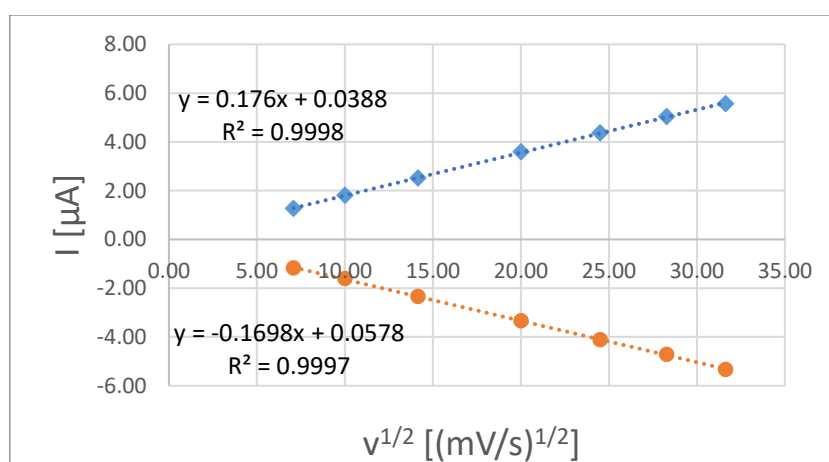
Figure S47: Plotted data of Randles-Sevcik-Equation Fe(MeOppz)$_3$ at different scan rates, first redox step

Table S13: Cyclovoltammetry data for Fe(MeOppz)$_3$ at different scan rates, second redox step

SCANRATE	[MV/S]	50	100	200	400	600	800	1000
E_{PC}	[V]	-0,268	-0,265	-0,265	-0,275	-0,268	-0,265	-0,265
E_{PA}	[V]	-0,207	-0,204	-0,197	-0,199	-0,197	-0,199	-0,207
$E_{1/2}$	[V]	-0,24	-0,23	-0,23	-0,24	-0,23	-0,23	-0,24
ΔE	[V]	0,061	0,061	0,068	0,076	0,071	0,066	0,059
I_{PC}	[µA]	-1,28	-1,72	-2,54	-3,62	-4,41	-5,05	-5,62
I_{PA}	[µA]	1,27	1,82	2,56	3,52	4,35	5,06	5,61
I_{PA}/I_{PC}		-0,99	-1,06	-1,01	-0,97	-0,99	-1,00	-1,00
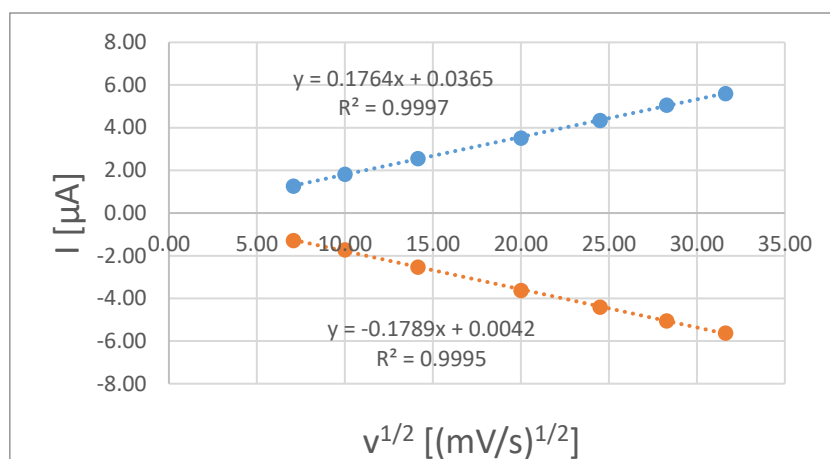
Figure S48: Plotted data of Randles-Sevcik-Equation Fe(MeOppz)$_3$ at different scan rates, second redox step

Table S14: Cyclovoltammetry data for Fe(MeOppz)$_3$ at different scan rates, second redox step

SCANRATE	[MV/S]	50	100	200	400	600	800	1000
E_{PC}	[V]	1,023	1,023	1,027	1,018	1,018	1,013	1,013
E_{PA}	[V]	1,091	1,088	1,096	1,093	1,103	1,103	1,106
$E_{1/2}$	[V]	1,06	1,06	1,06	1,06	1,06	1,06	1,06
ΔE	[V]	0,068	0,066	0,068	0,076	0,086	0,090	0,093
I_{PC}	[µA]	-1,29	-1,73	-2,10	-3,24	-3,84	-4,31	-4,72
I_{PA}	[µA]	0,94	1,38	1,90	2,71	3,27	3,67	4,05
I_{PA}/I_{PC}		-0,73	-0,80	-0,91	-0,84	-0,85	-0,85	-0,86
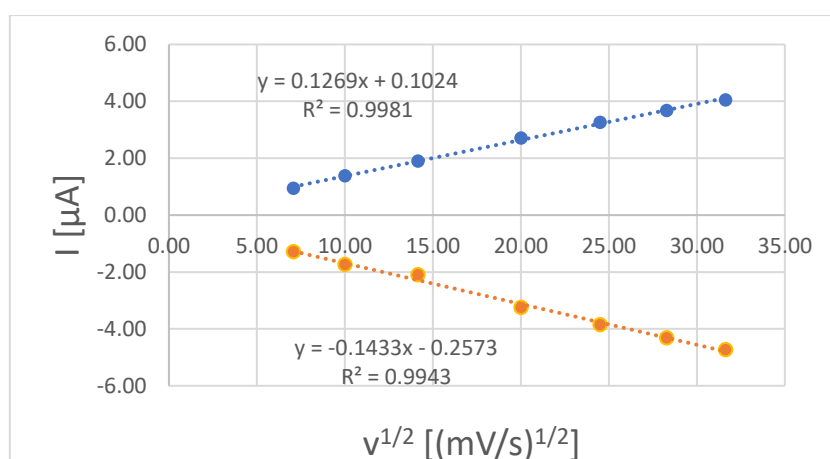
Figure S49: Plotted data of Randles-Sevcik-Equation Fe(MeOppz)$_3$ at different scan rates, third redox step
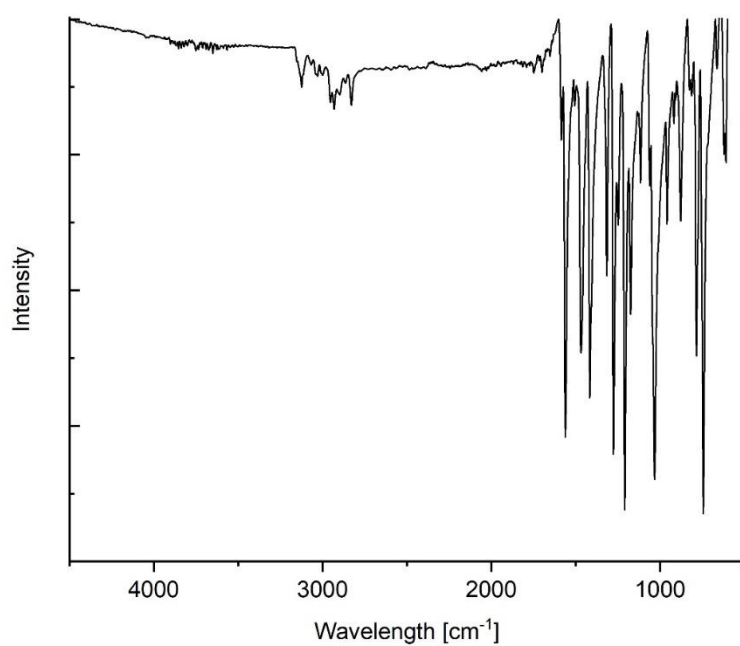
Figure S50: ATR-IR spectrum of complex Fe(MeOppz)$_3$

Illumination Experiments
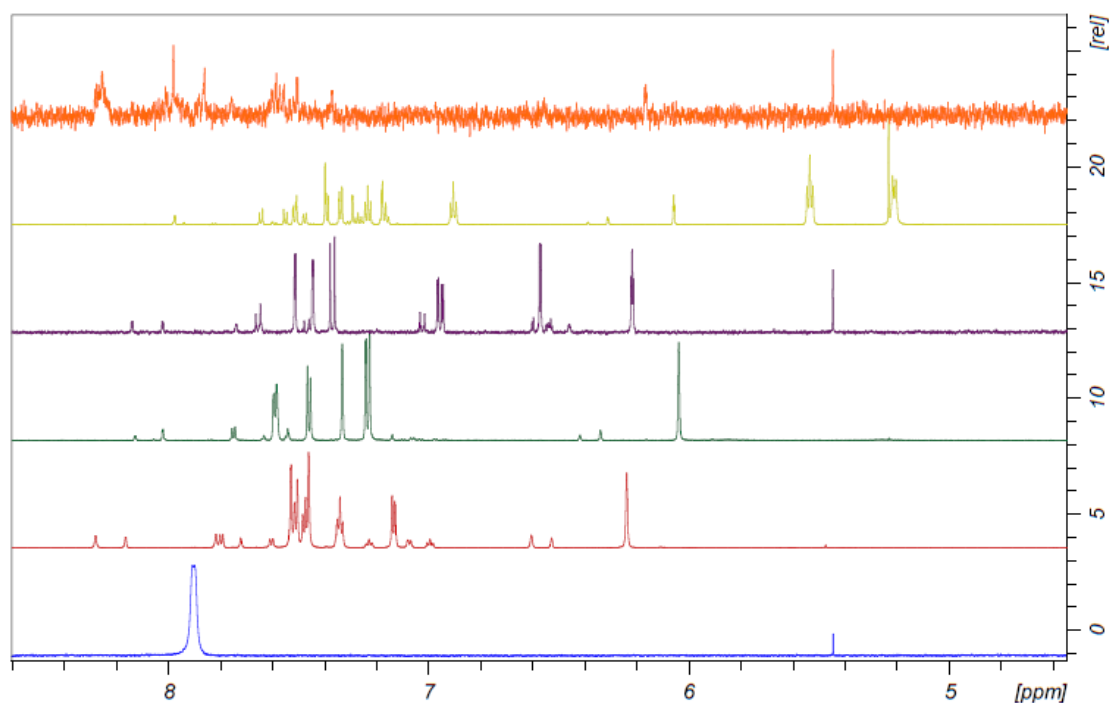
Figure S51: Experiments on complex stability in acetonitrile solution: before illumination of Fe(ppz)$_3$ (blue), after illumination of 24 h: Fe(ppz)$_3$ (red), Fe(CF$_3$ppz)$_3$ (green), Fe(MeOppz)$_3$ (purple), Fe(bppz)$_3$ (yellow), Fe)naphpz)$_3$ (orange, pure solubility decreases signal intensity)
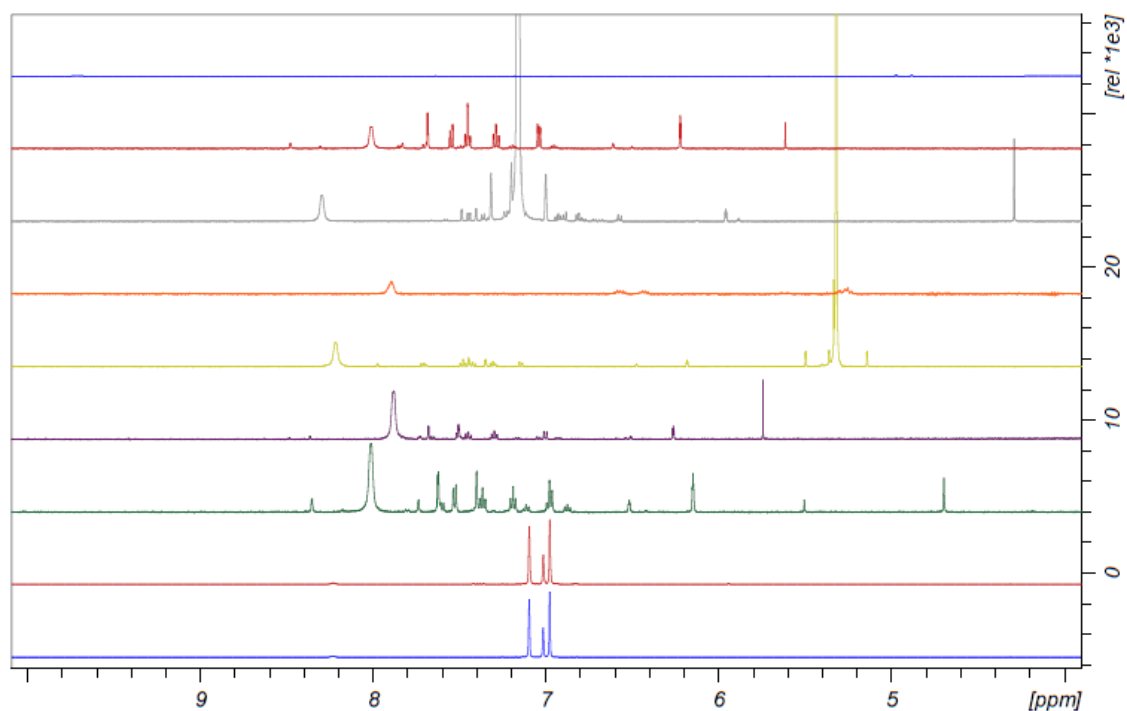
Figure S52: Experiments on complex stability exemplarily for Fe(ppz)₃, bottom blue: before illumination in toluene (blue), from there upwards after illumination: toluene (red), THF (green), DMSO (pruple), DCM (yellow), BuCN (orange), benzene (grey), acetone (red), 2Me-THF (blue).
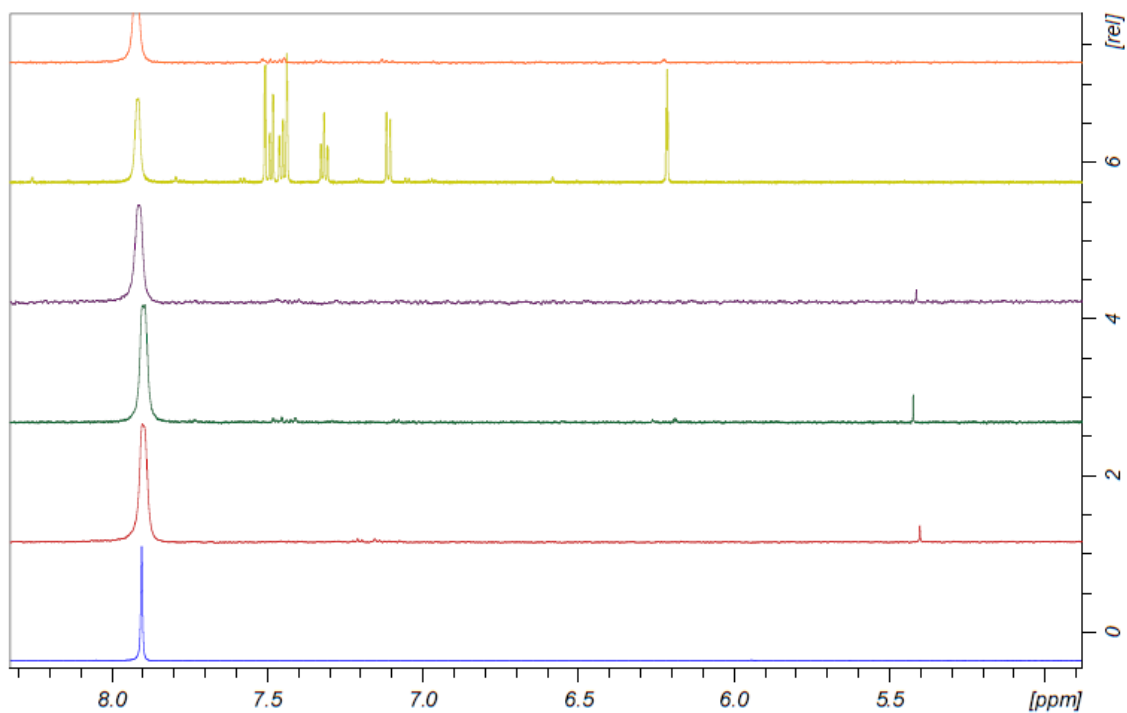
Figure S53: Decomposition of Fe(ppz)₃, with different filters. Blue: before irradiation; red: 320 nm bandwidth filter, green: 360 nm bandwidth filter, purple: 390 bandwidth filter; yellow: 400 longpass filter, orang: 495 longpassfilter. At 7.90 ppm complex signal, additional diamagnetic species in yellow spectra is the product of the reductive elimination.

33

Equation	y = a + b*x
Slope	-0.01442 ± 0.00143
Residual Sum of Squares	0.00131
R-Square (COD)	0.9619
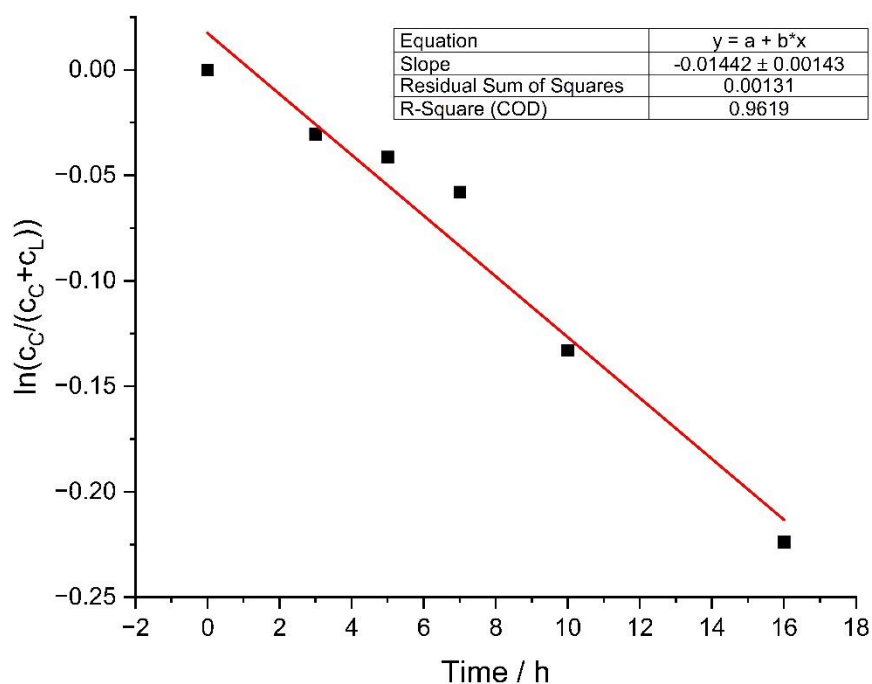
Figure S54: Calculated slope of the decomposition of Fe(ppz)$_3$, based on the relative intensities of TMS, the product of the reductive illumination at 6.21 ppm and the complex resonance at 7.90 ppm.

Computational

Table S15: Differential Gibbs free energy of PbEh-3c optimized structures excluding and including the SMD model for MeCN and BuCN implemented in ORCA. Negative values account for higher stability.

solvent	Δ Gibbs free energy [kcal/mol]		
	none	MeCN	BuCN
fac-Co(ppz)$_3$	0	-30.67	-32.05
fac-Fe(ppz)$_3$	0	-31.35	-32.73
Co(II) species	0	-58.16	-59.10
Fe(II) species	0	-58.9	-59.91

Table S16: Absolute an differential Gibbs free energy of PbEh-3c optimized structures of fac- and mer- isomers.

	Gibbs energy [kcal·mol^{-1}]		
	fac-isomer	*mer*-isomer	Δ(fac-mer)
Fe(naphpz)$_3$	-1946262.77	-1946262.19	-0.58
Fe(bppz)$_3$	-2092187.62	-2092186.16	-1.46
Fe(MeOppz)$_3$	-1872534.07	-1872536.20	2.13
Fe(CF$_3$ppz)$_3$	-2292413.78	-2292412.94	-0.84
Fe(ppz)$_3$	-1656600.74	-1656600.11	-0.63

Table S17: Comparison of the bond length and binding angles for the single crystal structure analysis and PBEh-3c geometry optimized fac-complexes.

complex	Experimental data			Computational data		
	Ø Fe-N [Å]	Ø Fe-C [Å]	∢ C-Fe-N [°]	Ø Fe-N [Å]	Ø Fe-C [Å]	∢ C-Fe-N$_{(ax)}$ [°]
Fe(naphpz)$_3$	2.0134(12)	1.9530(17)	169.99(7)	2.019	1.952	174.5
Fe(bppz)$_3$	2.0122(7)	1.9536(7)	172.90(1)	2.018	1.952	174.8
Fe(MeOppz)$_3$	2.0129(15)	1.9512(13)	170.89(5)	2.020	1.956	174.3
Fe(CF$_3$ppz)$_3$	2.0075(15)	1.9520(16)	170.46(6)	2.015	1.956	174.5
Fe(ppz)$_3$	2.0030(15)	1.9508(13)	171.54(7)	2.020	1.954	173.7
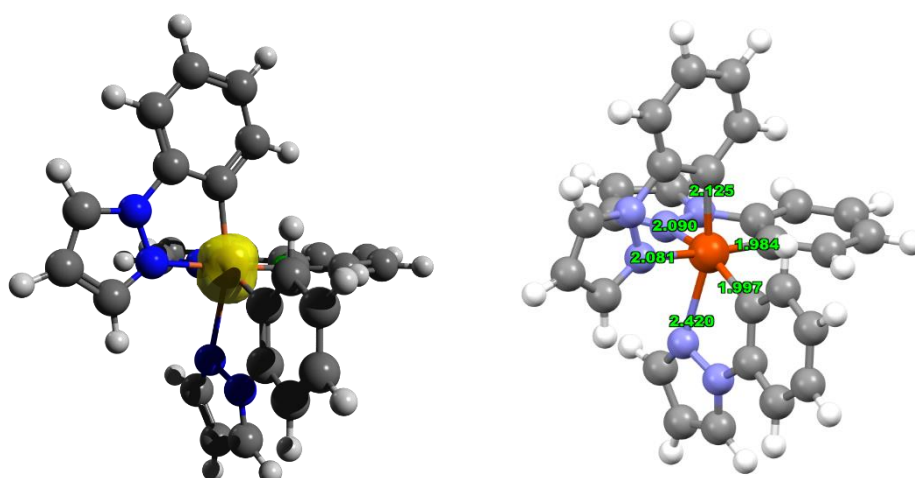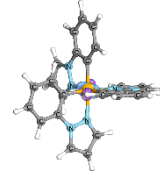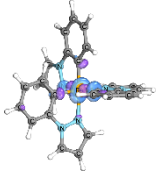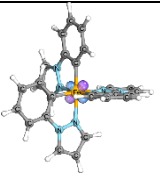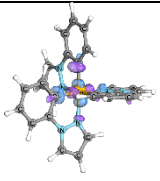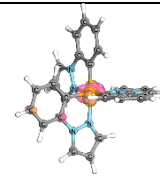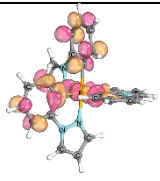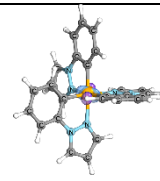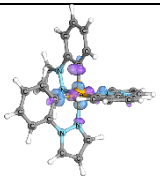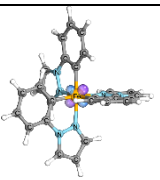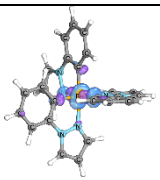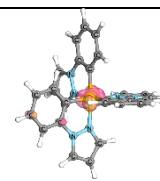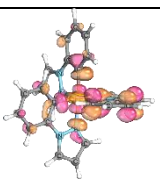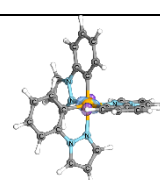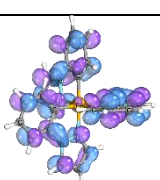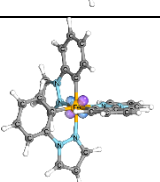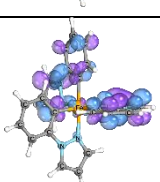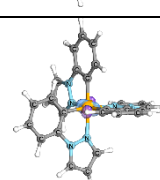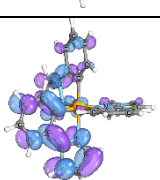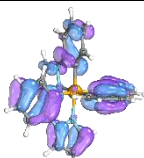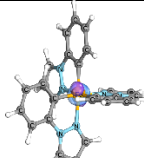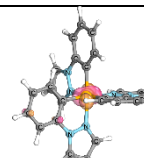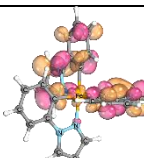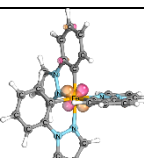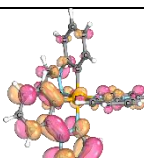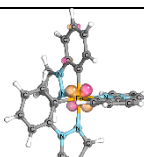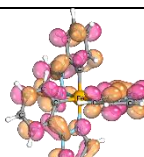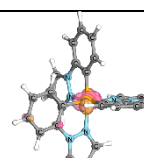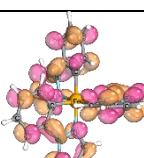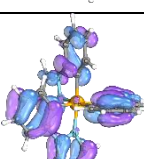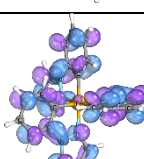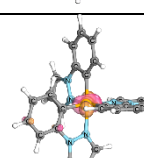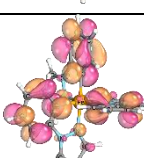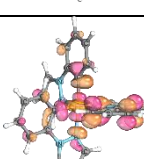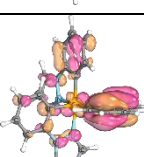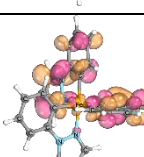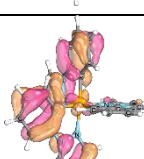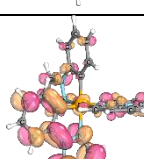
Figure S55: PBEh-3c optimized lowest quartet state of fac-**Fe(ppz)₃**. *Left*: Spin density plot. *Right*: Depicted Fe-ligand bond lengths.

| HOMO α | LUMO α | HOMO β | LUMO β |

Fe(ppz)₃

Fe(CF₃ppz)₃

Fe(MeOppz)₃

Fe(bppz)₃

Fe(naphpz)₃
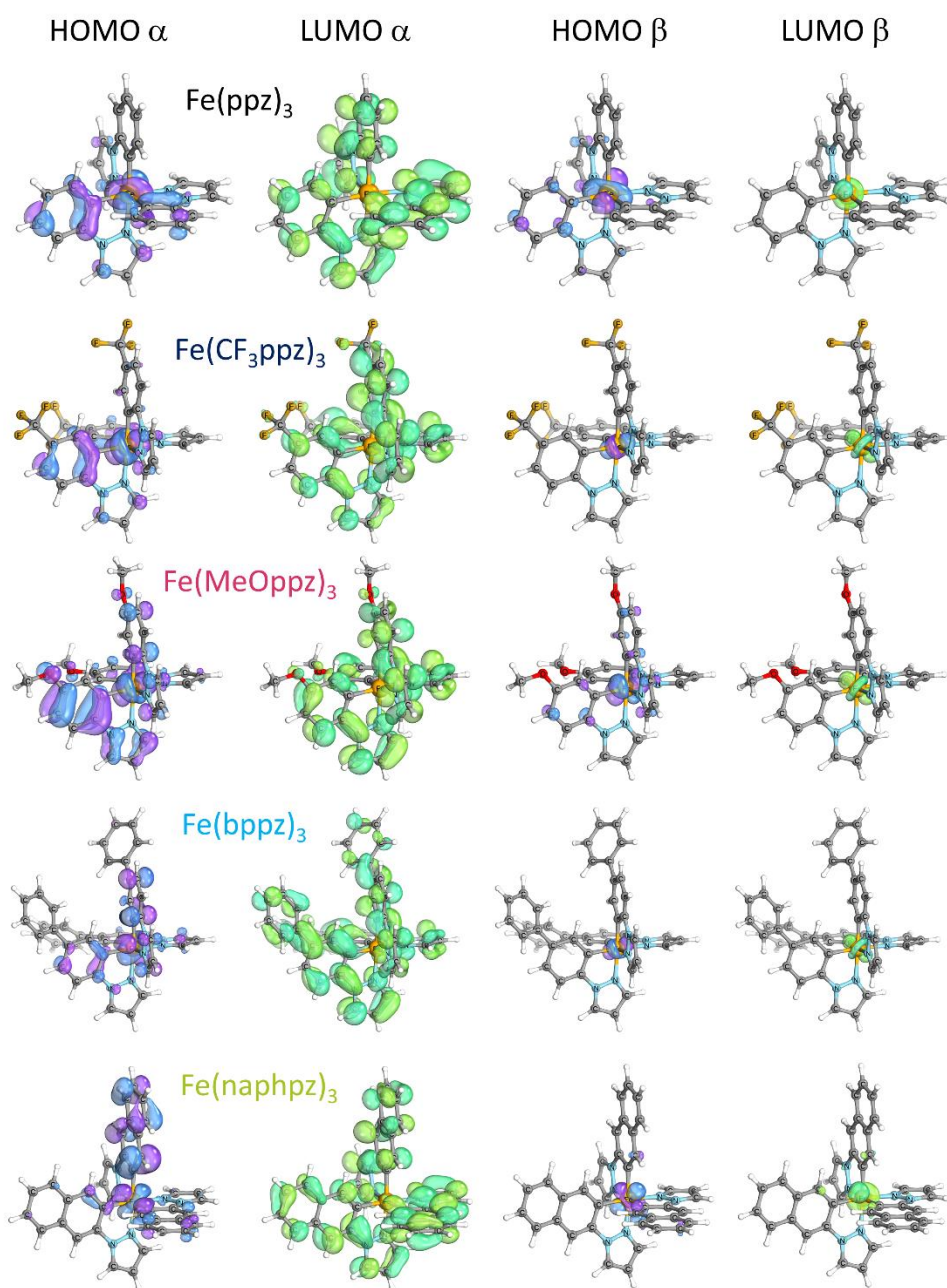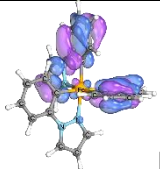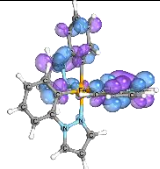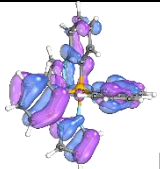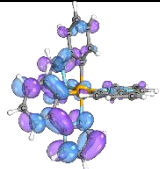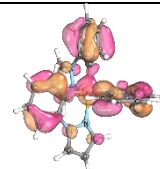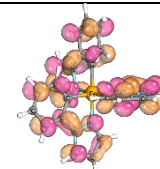
Figure S56: TPSSh/def2-TZVP calculated spatial distribution of the frontier orbitals of the respective complexes.

Table S18: Analysis of the main acceptor and donor orbital contribution to the TD-DFT calculated vertical transitions (Fig. 5) of fac-Fe(ppz)$_3$. The lettering of the transitions a-h refers to the assigned transitions in Fig. 5. Additionally, the calculated wavelength λ and oscillator strength f is given for the selected transitions.

Transition	Main Donor Orbitals	Main Acceptor Orbitals	Contribution to the transition
a λ = 451 nm, f = 0.0022	HOMO β	LUMO+8 β	13%
	HOMO-1 β	LUMO+7 β	11%
	HOMO α	LUMO+5 α	10%
b λ = 449 nm f = 0.0022	HOMO β	LUMO+7 β	13%
	HOMO-1 β	LUMO+8 β	11%
	HOMO α	LUMO+3 α	10%
c λ = 400 nm f = 0.0085	HOMO β	LUMO+1 β	84%
d λ = 388 nm f = 0.0128	HOMO-1 β	LUMO+3 β	30%
	HOMO β	LUMO+2 β	30%

d' *λ = 389 nm* *f = 0.0108*	HOMO-2 β	LUMO β	58%
e *λ = 351 nm* *f = 0.0159*	HOMO α	LUMO+3 α	15%
	HOMO-1 α	LUMO+1 α	12%
	HOMO-1 α	LUMO α	10%
f *λ = 346 nm* *f = 0.0251*	HOMO α	LUMO α	68%
g *λ = 281 nm* *f = 0.0328*	HOMO-2 β	LUMO+1 β	26%
	HOMO α	LUMO+5 α	16%
	HOMO-2 α	LUMO+3 α	7%
h *λ = 264 nm* *f = 0.2085*	HOMO-4 α	LUMO+2 α	10%
	HOMO-3 α	LUMO+1 α	9%

	HOMO-4 β		LUMO+3 β		7%
	HOMO-3 β		LUMO+2 β		7%
	HOM-5 α		LUMO α		6%

X-ray emission spectroscopy
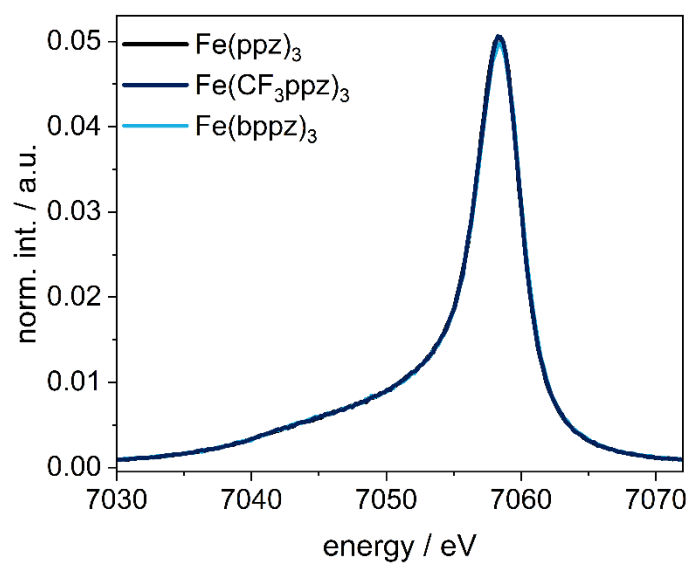
Figure S57: Experimental CtC spectra of Fe(ppz)$_3$, Fe(bppz)$_3$, Fe(CF$_3$ppz)$_3$ with different substituents.
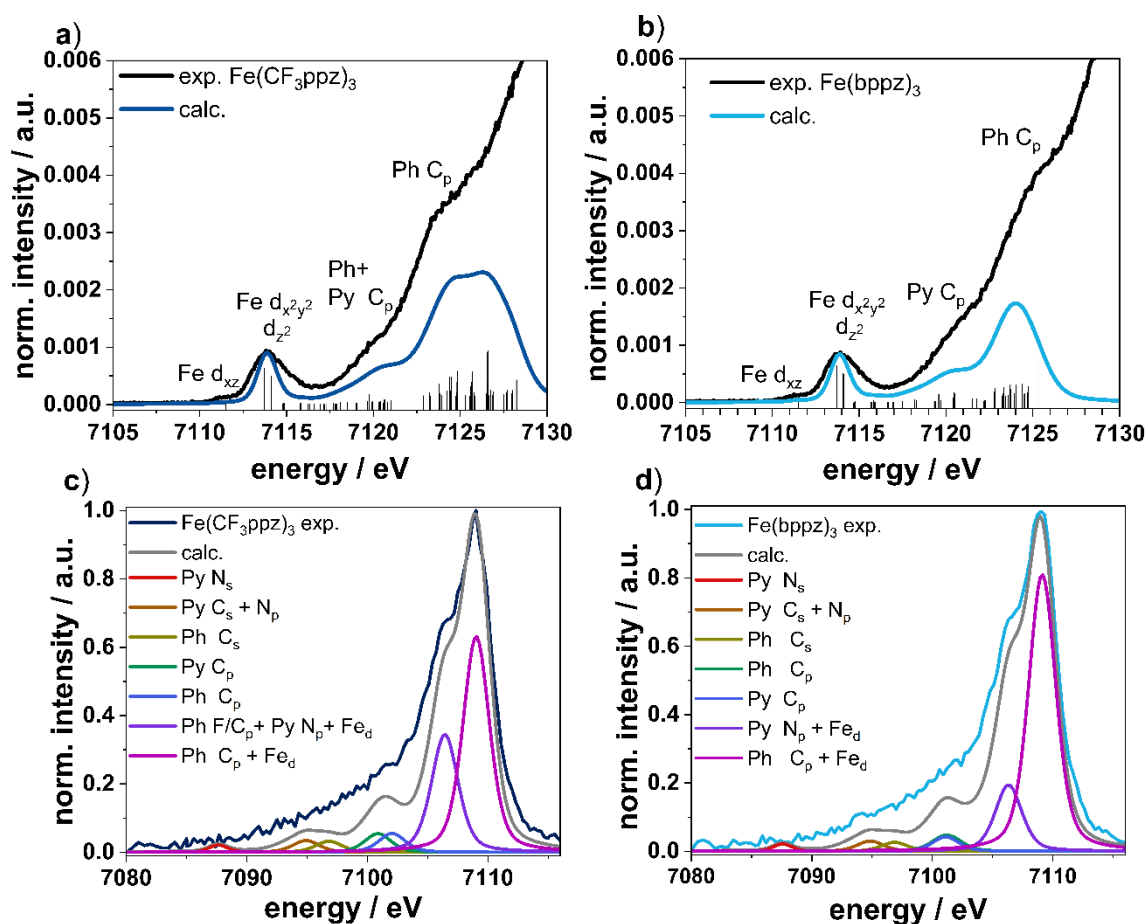
Figure S58: Comparison of experimental and calculated XANES (a, b) and VtC (c,d) spectra with main character of acceptor (a,b) and donor (c,d) orbitals orbital components for Pyrazol (Py) and Phenyl (Ph) accountable for the peak.

Single Crystal X-Ray Diffraction

The presented X-ray single crystal data were collected on a *Bruker Venture D8* three-cycle diffractometer equipped with a Mo K_α μ-source (λ=0.71073 Å). Monochromatization of the radiation was obtained using *Incoatec* multilayer Montel optics and a Photon III area detector was used for data acquisition. All crystals were kept at 120 K during measurement.

Data processing was carried out using the *Bruker* APEX 4 software package: This includes SAINT for data integration and SADABS for a multi-scan absorption correction. Structure solution was obtained by direct methods and the refinement of the structures using full-matrix least squares method based on F^2 were achieved in SHELX.[3,4] All non-hydrogen-atoms were refined anisotropically and the hydrogen atom positions were refined at idealized positions riding on the carbon atoms with isotropic displacement parameters $U_{iso}(H)$=1.2 $U_{eq}(C)$ resp. 1.5 U_{eq}(-CH_3) and C-H bond lengths of 0.93-0.96 Å. All CH_3 hydrogen atoms were allowed to rotate but not to tip.

Crystallographic data have been deposited at the Cambridge Crystallographic Data Centre assigned to the deposition numbers 2191100-2191104. Copies are available free of charge via www.ccdc.cam.ac.uk**.**

Crystallographic data

Tris(2-phenylpyrazolato-*N,C²*)iron(III) Fe(ppz)₃

CCDC number	2191100
Empirical formula	C55 H44 Cl2 Fe2 N12
Moiety formula	C27 H21 N6 Fe
Formula weight	1055.62 Da
Color	brown
Shape	needle
Temperature	119(2) K
Wavelength	0.71073 Å
Crystal system	Orthorhombic
Space group	$P2_12_12_1$
Unit cell dimensions	a = 13.6656(7) Å
	b = 15.4759(8) Å
	c = 22.6671(11) Å
Volume	4793.8(4) Å^3
Z	4
Density (calculated)	1.463 mg/m^3
Absorption coefficient	0.770 mm^{-1}
F(000)	2176
Crystal size	0.300 x 0.060 x 0.020 mm^3
Theta range for data collection	2.182 to 30.524°
Index ranges	-19≤h≤19, -22≤k≤22, -32≤l≤32
Reflections collected	144195
Independent reflections	14658 [R(int) = 0.0379]
Completeness to theta = 25.242°	99.8 %
Absorption correction	Semi-empirical from equivalents
Refinement method	Full-matrix least-squares on F^2
Data / restraints / parameters	14658 / 0 / 641
Goodness-of-fit on F^2	1.075
Final R indices [I>2σ(I)]	R1 = 0.0270, wR2 = 0.0694
R indices (all data)	R1 = 0.0321, wR2 = 0.0737
Absolute structure parameter	0.397(10)
Largest diff. peak and hole	0.499 e/Å^3 (0.51 Å from H223) and -0.367 e/Å^3 (0.52 Å from Fe1)
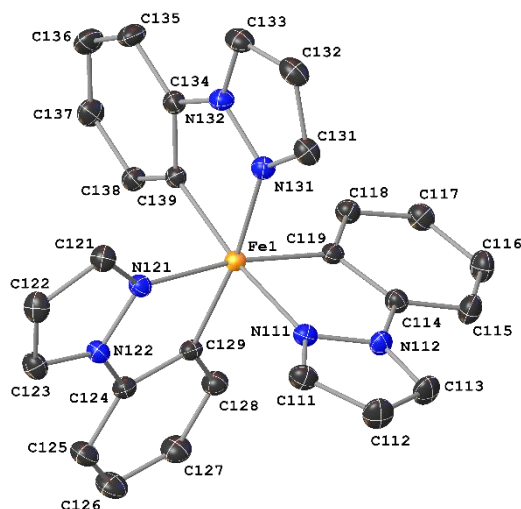
The structure was refined as an inversion twin (BASF=0.39746)

Tris(1-(([1,1'-biphenyl])-4-yl)phenyl)pyrazolato-*N,C²*)iron(III) Fe(bppz)₃

CCDC number	2191101
Empirical formula	C46.20 H35.40 Cl2.40 Fe N6
Moiety formula	C45 H33 Fe N6
Formula weight	815.53 Da
Color	red
Shape	prism
Temperature	120(2) K
Wavelength	0.71073 Å
Crystal system	Trigonal
Space group	R-3
Unit cell dimensions	a = 14.3819(5) Å
	b = 14.3819(5) Å
	c = 32.0647(16) Å
Volume	5743.7(5) Å^3
Z	6
Density (calculated)	1.415 mg/m^3
Absorption coefficient	0.605 mm^{-1}
F(000)	2528
Crystal size	0.200 x 0.200 x 0.180 mm^3
Theta range for data collection	2.833 to 36.372°
Index ranges	-23≤h≤24, -24≤k≤23, -53≤l≤53
Reflections collected	198137
Independent reflections	6215 [R(int) = 0.0423]
Completeness to theta = 25.242°	99.7 %
Absorption correction	Semi-empirical from equivalents
Refinement method	Full-matrix least-squares on F^2
Data / restraints / parameters	6215 / 0 / 157
Goodness-of-fit on F^2	1.046
Final R indices [I>2σ(I)]	R1 = 0.0332, wR2 = 0.0909
R indices (all data)	R1 = 0.0368, wR2 = 0.0940
Largest diff. peak and hole	0.538 e/Å^3 (0.65 Å from C4) and -0.355 e/Å^3 (0.53 Å from Fe1)
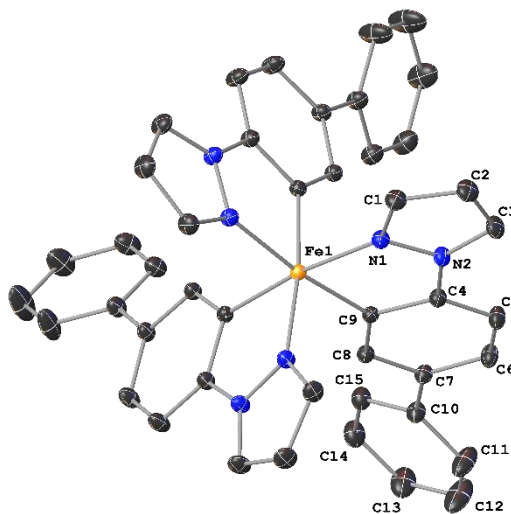
For refinement, two partially occupied dichloromethane molecules were treated with SQUEEZE from the PLATON software package.[5]

Tris(1-(4-(trifluoromethyl)phenyl)pyrazolato-*N,C²*)iron(III) Fe(CF₃ppz)₃

|	
CCDC number	2191102
Empirical formula	C67 H44 F18 Fe2 N12
Moiety formula	C30 H18 F9 Fe N6
Formula weight	1470.84 Da
Color	yellow
Shape	plate
Temperature	120(2) K
Wavelength	0.71073 Å
Crystal system	Triclinic
Space group	P-1
Unit cell dimensions	a = 13.5555(9) Å
	b = 16.6300(10) Å
	c = 16.8788(10) Å
	α= 104.514(2)°
	β= 108.952(2)°
	γ = 109.287(2)°
Volume	3111.8(3) Å³
Z	2
Density (calculated)	1.570 mg/m³
Absorption coefficient	0.575 mm⁻¹
F(000)	1488
Crystal size	0.100 x 0.100 x 0.020 mm³
Theta range for data collection	2.339 to 32.121°
Index ranges	-20≤h≤20, -24≤k≤24, -25≤l≤25
Reflections collected	314702
Independent reflections	21751 [R(int) = 0.0566]
Completeness to theta = 25.242°	99.9 %
Absorption correction	Semi-empirical from equivalents
Refinement method	Full-matrix least-squares on F²
Data / restraints / parameters	21751 / 163 / 987
Goodness-of-fit on F²	1.080
Final R indices [I>2σ(I)]	R1 = 0.0447, wR2 = 0.1024
R indices (all data)	R1 = 0.0694, wR2 = 0.1226
Largest diff. peak and hole	1.147 e/Å³ (0.77 from F21D) and -0.789 e/Å³ (0.49 Å from F12I)
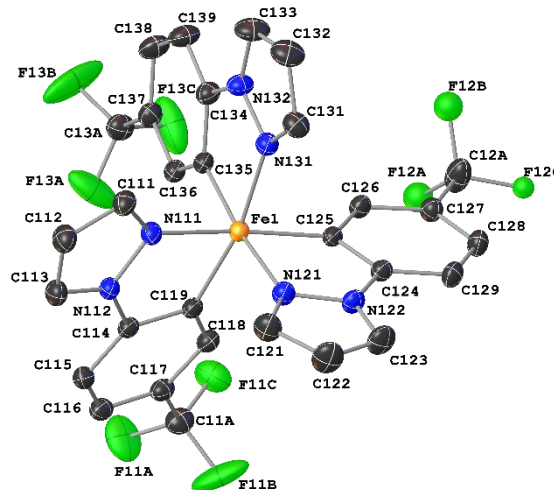
The asymmetric unit of the structure contains two complex molecules. Four CF₃-groups tend to rotate and could be refined splitted in two positions, a fifth one in three positions. Due to this disorder, not all splitted atom groups could be refined anisotropically.

Tris(1-(naphthalen-2-yl)pyrazolato-*N,C²*)iron(III) Fe(naphpz)₃

CCDC number	2191103
Empirical formula	C52 H37 Fe N8
Moiety formula	C39 H27 Fe N6
Formula weight	829.74 Da
Color	orange
Shape	plate
Temperature	120(2) K
Wavelength	0.71073 Å
Crystal system	Monoclinic
Space group	P2₁/n
Unit cell dimensions	a = 11.3521(10) Å
	b = 30.655(3) Å
	c = 12.3313(11) Å
	β= 110.723(2)°
Volume	4013.7(6) Å³
Z	4
Density (calculated)	1.373 mg/m³
Absorption coefficient	0.425 mm⁻¹
F(000)	1724
Crystal size	0.280 x 0.180 x 0.100 mm³
Theta range for data collection	2.030 to 30.546°
Index ranges	-16≤h≤16, -43≤k≤43, -17≤l≤17
Reflections collected	190973
Independent reflections	12271 [R(int) = 0.0682]
Completeness to theta = 25.242°	99.9 %
Absorption correction	Semi-empirical from equivalents
Refinement method	Full-matrix least-squares on F²
Data / restraints / parameters	12271 / 0 / 550
Goodness-of-fit on F²	1.131
Final R indices [I>2σ(I)]	R1 = 0.0455, wR2 = 0.1075
R indices (all data)	R1 = 0.0734, wR2 = 0.1274
Largest diff. peak and hole	1.196 e/Å³ (0.63 Å from H405) and -0.698 e/Å³ (0.69 Å from Fe1)
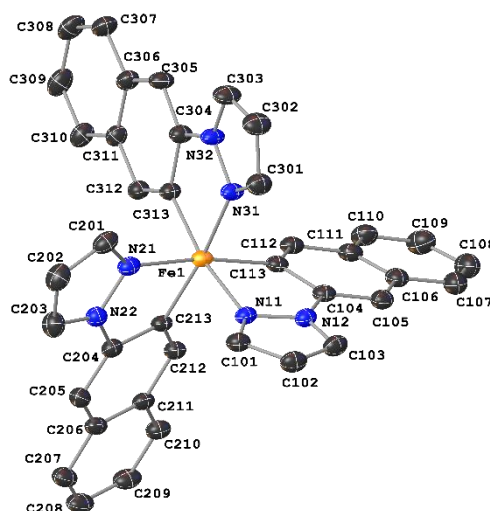
Tris(1-(4-methoxyphenyl)pyrazolato-*N,C²*)iron(III) Fe(MeOppz)$_3$

CCDC number	2191104
Empirical formula	C30 H27 Fe N6 O3
Moiety formula	C30 H27 Fe N6 O3
Formula weight	575.42 Da
Color	red
Shape	block
Temperature	120(2) K
Wavelength	0.71073 Å
Crystal system	Trigonal
Space group	R-3
Unit cell dimensions	a = 19.9138(11) Å
	b = 19.9138(11) Å
	c = 48.704(4) Å
Volume	16727(2) Å^3
Z	24
Density (calculated)	1.371 mg/m^3
Absorption coefficient	0.584 mm^{-1}
F(000)	7176
Crystal size	0.18 x 0.18 x 0.10 mm^3
Theta range for data collection	2.400 to 32.048°
Index ranges	-29≤h≤29, -29≤k≤29, -72≤l≤72
Reflections collected	660843
Independent reflections	12775 [R(int) = 0.0674]
Completeness to theta = 25.242°	96.8 %
Absorption correction	Semi-empirical from equivalents
Refinement method	Full-matrix least-squares on F^2
Data / restraints / parameters	12775 / 0 / 505
Goodness-of-fit on F^2	1.143
Final R indices [I>2σ(I)]	R1 = 0.0350, wR2 = 0.0834
R indices (all data)	R1 = 0.0530, wR2 = 0.0997
Largest diff. peak and hole	0.701 e/Å^3 (2.28 Å from H13D) and -0.556 e/Å^3 (0.64 Å from Fe1)
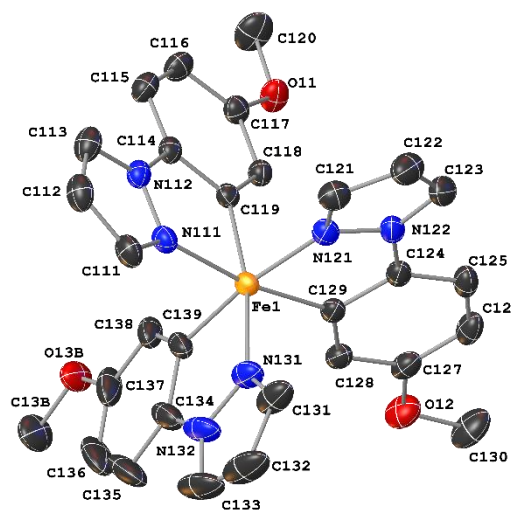
One methoxy group of the structure is disordered over two positions and could be refined anisotropically. Furthermore, two water molecules are only partially occupied (SOF<0.2), could not be refined and were therefore treated using SQUEEZE from the PLATON software package.[5]

References

(1) Cristau, H.-J.; Cellier, P. P.; Spindler, J.-F.; Taillefer, M. Mild Conditions for Copper-Catalysed *N*-Arylation of Pyrazoles. *Eur. J. Org. Chem.* **2004**, *2004* (4), 695–709. DOI: 10.1002/ejoc.200300709.

(2) Cristau, H.-J.; Cellier, P. P.; Spindler, J.-F.; Taillefer, M. Highly efficient and mild copper-catalyzed N- and C-arylations with aryl bromides and iodides. *Chem. Eur. J.* **2004**, *10* (22), 5607–5622. DOI: 10.1002/chem.200400582.

(3) Sheldrick, G. M. Crystal structure refinement with SHELXL. *Acta crystallographica. Section C, Structural chemistry* **2015**, *71* (Pt 1), 3–8. DOI: 10.1107/S2053229614024218. Published Online: Jan. 1, 2015.

 (4) Sheldrick, G. M. SHELXT - integrated space-group and crystal-structure determination. *Acta crystallographica. Section A, Foundations and advances* **2015**, *71* (Pt 1), 3–8. DOI: 10.1107/S2053273314026370. Published Online: Jan. 1, 2015.

 (5) Spek, A. L. PLATON SQUEEZE: a tool for the calculation of the disordered solvent contribution to the calculated structure factors. *Acta crystallographica. Section C, Structural chemistry* **2015**, *71* (Pt 1), 9–18. DOI: 10.1107/S2053229614024929. Published Online: Jan. 1, 2015.